Towards optical detection of a single electron

Moradi, A.

Citation

Moradi, A. (2021, February 23). *Towards optical detection of a single electron. Casimir PhD Series*. Retrieved from https://hdl.handle.net/1887/3149275

Cover Page

Universiteit Leiden

Leiden University
Repository

Author: Moradi, A.
Title: Towards optical detection of a single electron
Issue Date: 2021-02-23

3

Laser-induced frequency tuning of fourier-limited single-molecule emitters

The local interaction of charges and light inorganic solids is the basis of distinct and fundamental effects. We here observe, at the single-molecule scale, how a focused laser beam can locally shift by hundreds of times their natural line width and, in a persistent way, the transition frequency of organic chromophores cooled at liquid helium temperature in different host matrices. Supported by quantum chemistry calculations, the results can be interpreted as effects of a photoionization cascade, leading to a stable electric field, which Stark shifts the molecular electronic levels. The experimental observation is then applied to a common challenge in quantum photonics, i.e., the independent tuning and synchronization of close-by quantum emitters, which is desirable for multiphoton experiments. Five molecules that are spatially separated by about $50\mu m$ and originally $20GHz$ apart are brought into resonance within twice their line width. This tuning method, which does not require additional fabrication steps, is here independently applied to multiple emitters, with an emission line width that is only limited by the spontaneous decay and an inhomogeneous broadening limited to $1nm$. The system hence shows promise for photonic quantum technologies.

3.1. Introduction

Single fluorescent molecules of polycyclic aromatic hydrocarbons (PAHs) embedded in crystalline organic matrices are widely considered highly coherent, stable, and bright two-level quantum systems in the solid state.[1–5] Indeed, they can be operated as single-photon sources,[6] combining high count rate and Fourier-limited line widths,[7–9] or as nanoprobes with exquisite sensitivity to electric fields, pressure, and strain.[10,11] PAH-based quantum devices can also be readily integrated in photonic chips.[12–15] A major advantage of PAH systems resides in the possibility to mass produce nominally identical fluorescent molecules at low costs and still obtain outstanding optical and optoelectronic properties. PAHs are under investigation for their use also in organic solar cells,[16] as well as in super-resolution microscopy methods.[17] Furthermore, the Stark effect is a well-established technique for tuning the molecular transitions.[18–20] Broad tunability has been demonstrated for instance in the case of anthracene nanocrystals (Ac NCXs) doped with dibenzoterrylene (DBT) molecules, exhibiting a quadratic Stark shift upon the application of a voltage bias (tuning range $> 400\,GHz$, comparable to the inhomogeneous broadening).[21] Also a large linear and homogeneous Stark shift has been achieved, embedding DBT in 2,3-dibromonaphthalene (DBN), suggesting the system as a promising nanoprobe of electric fields and charges.[22] Such previous results demonstrate the potential of molecular-based techniques which, in principle, could also go beyond single-emitter devices. However, current tuning methods have to be scaled up, allowing for local control of the transition frequency. This is crucial to optimize coupling of multiple emitters to photonic structures, as well as quantum interference among distinct sources on chip. To this purpose, electrical tuning of the emission wavelength for multiple sources is challenging to implement. Optical control might instead enable simple, fast, and independent frequency tuning of separated emitters. Recent promising works have shown laser-induced frequency tuning of epitaxial quantum dots' transitions. Physical manipulation of the sample is in this case confined within the laser beam diameter, and localized tuning of the emitters is achieved *via* thermal annealing,[23] mechanical expansion through phase-change materials,[24] or controlled strain through the host/substrate medium[25] Nevertheless, the observed decoherence and spectral diffusion of the emitters' line width can be detrimental in many applications.

In this work we demonstrate fabrication-free, micron-resolved, optical frequency tuning of individual DBT molecules. We attribute the laser-induced frequency tuning of the molecular zero-phonon line (ZPL) to a local Stark shift, associated with optically induced long-lived charge-separated states, which notably persists for at least several hours after the pump laser is switched off. We first demonstrate the versatility of the concept, studying DBT in two different types of molecular crystals. A full characterization of the laser-induced frequency tuning is presented. In particular, we show how the magnitude of the induced spectral shift can be extended over a broad frequency range, by acting on the pump laser parameters. We also verify that close-to-Fourier-limited emission and photostability are preserved at cryogenic temperatures after the tuning process. In the following section, we demonstrate the scalability of the presented method as we show

independent tuning of individual emitters down to $15\,m$ in proximity. In particular, we prove that the method can be extended to the frequency scale of the inhomogeneous line broadening, achieving spectral shifts that are more than 3 orders of magnitude larger than the natural line width. We show ZPL frequency matching (within two linewidths) of five molecular emitters, all within a $50 \times 50\,\mu m$ area and initially $> 20\,GHz$ apart in frequency. Finally, we propose a model based on the photoionization mechanism of charge generation and support it with low-level quantum chemistry calculations. Different routes for the charge generation process, which may be an alternative or concurrent to the one described by our model, are also briefly discussed.

Overall, the possibility of using an all-optical approach to shift the transition frequency of individual emitters while maintaining coherent spectral properties offers a promising tool for applications in quantum nanophotonics. In particular, the presented results will benefit the realization of scalable quantum photonic devices and protocols based on multiple photons and multiple single-molecule emitters. More generally, the concept of laser-induced charge separation via photo-ionization of molecules can have broader scope in applications of single-molecule emitters, for example in nanoscale sensing of charge-carrier generation and in understanding the photo-conductivity and photorefraction of organic semiconductors.

3.2. Methods

3.2.1. Sublimation growth of DBT:DBN Single Crystals

2,3-Dibromonaphthalene used in this work was purchased from Ark Pharm Inc. High-quality single crystals of zone-refined DBN doped with dibenzoterrylene molecules were obtained by co-sublimation at ~ 0.2 bar of argon gas. To prevent perturbations from the convection flow in the sublimation chamber, the sublimator was kept horizontal during growth. The sublimation-grown crystals develop along the (a,b) plane as thin mm-sized plates or flakes, with a typical thickness of a few microns along the c-axis.

3.2.2. Preparation of DBT:Ac nanocrystals

Nanocrystals (NCs) of anthracene doped with a single-molecule concentration of DBT are grown by injecting $100\,\mu L$ of a $4{:}107$ mixture of 1 mM DBT−toluene and 5 mM Ac−acetone solutions into 2 mL of sonicating Milli-Q water. After 30 min of sonication, solvents are completely dissolved and DBT:Ac NCs are formed as an aqueous suspension (for more details see ref S1). The nanocrystals are then deposited on the substrate via drop-casting of $\sim 10\,\mu L$ of the suspension followed by desiccation. In particular, the substrates employed in the experiment are simple glass coverslips and coverslips coated with sputtered gold (film thickness of ~ 200 nm). After the deposition, NCs are protected from sublimation by spin-coating a 200 nm thick layer of poly(vinyl alcohol) (PVA). Solvents Ac and PVA were purchased from Sigma- Aldrich, water was deionized by a Milli-Q Advantage A10 system (resistivity of $18.2\,M\Omega \times$ cm $at\,25\,°C$), and DBT was purchased from Mercachem.

3.2.3. Optical microscopy (DBT:DBN)

All single-molecule measurements with DBT:DBN crystals were done at 1.2 K in a home-built-liquid-helium bath cryostat. Single crystals of DBT:DBN were optically attached to a glass substrate containing interdigitated gold markers previously deposited by lithography, which served to locate different parts of the single crystal in consecutive experiments. All pump excitation experiments on DBT:DBN were performed on the crystal parts that were in contact with the glass substrate. Single DBT molecules were excited by a tunable continuous-wave Ti:sapphire laser (M Squared) at around 756.7 ± 0.2 nm. This laser is denoted in the text as a probe (laser) beam. The frequency range of typically $10 GHz$ was scanned with 1000 points and 5 ms integration time per point, with a typical power of 0.3 to 0.7 μW focused on the sample. The output of the laser was continuously monitored by an external Fabry−Perrot cavity. The response of this cavity was used to monitor the laser frequency drift in real time and to compensate for a small nonlinearity of the frequency scan. A second, more intense (pump) laser beam was used to induce spectral shifts in DBT:DBN crystals. The laser light was produced by a Coherent ring laser, operated with rhodamine 101 (640) dye and pumped with a 532 nm solid-state laser. The operating wavelength of the pump laser was at around $631nm$, and a typical power focused on the sample was 10μW to 5 mW. In all experiments the sample was scanned with either only a probe laser (756.7 nm) or simultaneously with both pump (631 nm) and probe lasers focused on the sample. The sample was scanned in a confocal epi-fluorescence arrangement using a scanning mirror (Newport, FSM-300-01). A $\lambda/4$ wave plate was used to produce a circularly polarized beam for more efficient excitation of single DBT emitters. The fluorescence light was collected by a cryogenic objective (Microthek, $NA = 0.8$) and detected by a single-photon counting module (Excelitas SPCM-AQRH-16) with a set of filters (Chroma HQ760LP and Semrock FF02-809/81) in the detection path.

3.2.4. Optical microscopy (DBT:Ac)

The optical characterization of individual DBT molecules in Ac NCs was performed with a home-built scanning fluorescence confocal microscope. All measurements were done at about 3.5 K, with the sample in a closed-cycle helium cryostat (Cryostation by Montana Instruments). The transition line width of individual molecules was measured under confocal resonant excitation, with a CW distributed feedback diode laser (Toptica, LD-0785-0080-DFB-1), named probe, which is centered at 784.6 nm and can be scanned continuously in frequency over a range of $800 GHz$. Frequency shifts of molecules emission were generally induced in off-resonant configuration by using a CW external-cavity diode laser (Toptica, DLX110), named pump, centered at 767 nm and operated at higher power (also in confocal mode). In particular, the laser frequency can be tuned through fine tilting of the Bragg grating of the diode source, enabling mode-tuning within about ± 4 nm around the central value. Laser-induced shifting was also performed by using the probe laser operated at higher power. All laser sources were fiber-coupled and linearly polarized by means of a half- wave plate in the excitation path to allow for optimal

coupling to the single molecules' linear dipole. The excitation light was focused onto the sample by a glass-thickness-compensation air objective (OptoSigma $50 \times$, $NA = 0.67$, $WD = 10.48$ mm) and scanned over the sample by a telecentric system and a dual-axis galvo-mirror. The Stokes-shifted fluorescence was hence separated from the excitation light through a dichroic mirror (Semrock FF776-Di01) and a long-pass filter (Semrock RazorEdge LP02-785RE-25) and detected by either an EMCCD camera (Andor iXon $885, 1004 \times 1002$ pixels, pixel size 8 mm $\times$ 8 mm), for measuring fluorescence space-maps and spectral properties, or by a SPAD (SPCM-AQRH-14-TR by Excelitas). A converging lens was inserted in the excitation path, just before the dichroic mirror, to switch between confocal and wide-field illumination. For the antibunching measurement shown in the SI, we employed a Hanbury-Brown and Twiss configuration, based on a fibered beam splitter, two fiber-coupled SPADs (SPCM-800-14-FC by Excelitas), and a time-correlated single-photon counting (TCSPC) card (PicoHarp 300 by PicoQuant). Fiber-coupling of the single-molecule fluorescence was achieved by means of an adjustable fiber-collimator and a free-space telescope for mode-matching.

3.3. Results and discussions

The optically induced frequency tuning of light emission is studied via single-molecule measurements on DBT chromophores embedded in two different host systems, namely, anthracene (Ac) nanocrystals doped with low DBT concentration ($\sim 10^{-2} molecules/GHz$) and DBN crystal flakes, doped with high DBT concentration ($\sim 1 molecule/GHz$). The molecular components of the two studied systems and their electronic energy levels are summarized in Figure 3.1.a. We also report additional results on a third system of DBT in naphthalene in the SI, showing that the effect applies to a broader range of organic crystals. The studied systems share the same guest molecule (DBT) but are known to have different response to the electric field. In particular, DBT:DBN exhibits a large linear Stark coefficient due to the broken inversion symmetry of guest DBT molecules,[22] while DBT:Ac shows a quadratic Stark coefficient.[7,21]

All the experiments are performed at liquid helium temperatures. In these conditions, the purely electronic ZPL is about $40\ to\ 60\ MHz$ wide. The spectral line shape can be traced with a standard epifluorescence microscope by scanning the frequency of the CW excitation laser (named "probe" hereafter) around the resonant wavelength. The Stokes-shifted fluorescence, spectrally selected through a long-pass filter, is correspondingly measured with an avalanche photodiode, giving access to the excited state occupation probability as a function of the excitation wavelength.

Optical frequency tuning of the narrow-band ZPL is achieved by focusing on the target crystalline regions a second CW laser (named "pump" hereafter), generally operating at a different wavelength and higher intensity. In Figure 3.1.b,c, real-time information on the laser-induced shift is provided by color maps showing, as a function of time, the excitation spectra of DBT molecules, exposed to the pump laser for a long time interval. In Figure 3.1.a, simplified Jablonski diagrams are outlined, showing the energies of the

pump as well and probe lasers employed in the experiments. The probe laser is scanned over the ZPL transitions around 785 nm for DBT:Ac (Figure 3.1.b) and $756\,nm$ for DBT:DBN (Figure 3.1.c), whereas the pump laser is centered at 765.8 and $630\,nm$, respectively.
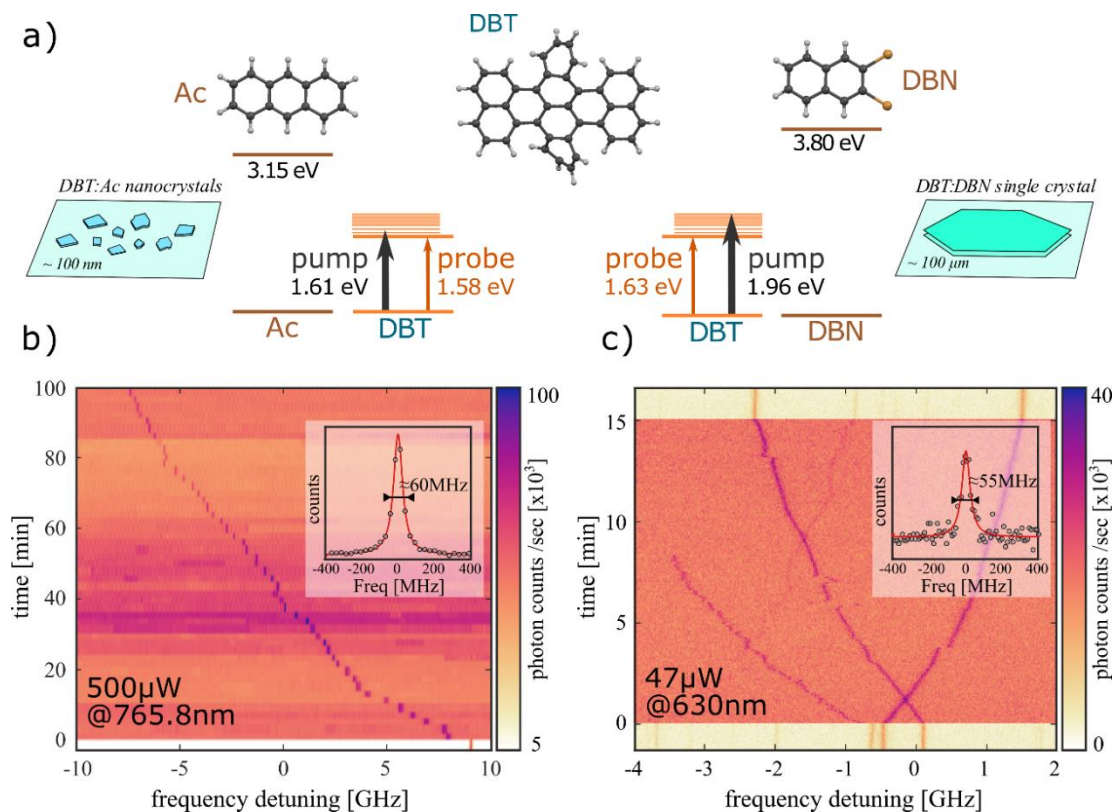

Figure 3.1: a) Chemical structures of the guest (DBT) and host molecules (Ac, DBN) used in this study. The energies of the pump and probe beams used in the experiments are indicated for comparison. Laser-induced frequency shift for DBT in Ac (b) and DBT in DBN (c). The fluorescence count rate is plotted in color scale as a function of the excitation laser frequency, scanning over the molecular ZPL. The measurements are repeated in time, while the pump laser is switched on. The pump presence is recognized by the onset of a strong background signal; that is, the light-yellow background represents scans without the pump beam. Insets in panels (b) and (c) represent horizontal cuts and include the Lorentzian fits to the data.

Zero-phonon lines corresponding to different molecules can thus be initially identified, followed during the burst duration above the background fluorescence, and recovered at different frequency positions after the exposure (Figure 3.1.c). It is worth noticing that after the pump laser illumination DBT molecules preserve excellent spectral stability and close-to-lifetime limited resonance line width. In particular, the spectral width amounts to ~ 60 and $\sim 55 MHz$ for DBT:Ac and DBT:DBN, respectively (see insets in Figure 3.1). In the first case, the line broadening, compared to before the shift procedure, is unchanged and is attributed to the higher temperature of about $3.5K$ at which the experiment is held. Spectral wandering is present in these samples and is related to the fluctuations of the local electric field, due to charge migrations. The energy shift in DBT emission persists even after the pump is turned off for about 24h, ruling out the hypothesis of temporary heating effects. Furthermore, the frequency incre- ment after each probe

scan (single row in the color map), on the order of a few line widths, hints at the possibility of a fine calibration of the effect, which is analyzed in more details in the following sections.

The number of DBT molecules exposed to the laser confocal illumination (beam diameter $d \approx 1\mu m$) is different in the two host−guest systems. On a sample of distributed DBT:Ac NCX (Figure 3.1.b), a single nanocrystal can be isolated within the beam area, which implies that typically only one molecule is resonant within a $500 GHz$ scan of the probe. However, this cannot exclude the presence of broader molecules on the surface that could be weakly resonant with the intense pump laser. The reported frequency shift is always toward longer wavelengths, in agreement with the characteristic quadratic Stark effect of DBT in Ac. [21] On the other hand, within the highly doped DBN flakes, the confocal volume typically contains several chromophores within a $10\ GHz$ scan of the probe-laser frequency. As reported in Figure 3.1.c, shifts with opposite signs are observed within the sample of DBT:DBN, for which a large linear Stark coefficient has been reported. [22]

Importantly, although each individual molecule may sense slightly different local electric fields (see the SI for more information), the fairly homogeneous response of most emitters in this well-defined system indicates that the laser-induced effect acts on all emitters within the diffraction-limited volume. These results jointly corroborate the interpretation of a laser-induced electric field buildup, leading to a Stark effect.

It is worth noticing that, when the pump is switched on, the measurements exhibit a strong background signal, which scales linearly with power. This light might be due to the presence of several DBT molecules within the illumination volume in the host matrices, weakly excited by the high-power pump laser. We note that such background shows much higher variability in the case of DBT:Ac than for DBT:DBN (Figure 3.1.b,c), as expected, since fewer molecules are involved in the former system. The role of nearby nonresonant DBT molecules in the shifting mechanism is thoroughly discussed further in the manuscript and in the Supporting Information. Notably, the emission purity for single-photon-based applications is not compromised by such background levels (see SI, Figure S3.3), since the pump power employed for single-photon source operation is much lower than that used to shift the ZPL frequency, yielding a negligible background level. [26] In particular, the statistical analysis of $g^{(2)}(t)$ measurements on 40 DBT:Ac nanocrystals performed in our previous work [27] yields a single-photon purity higher than 97% for 82% of the cases. In the following, we discuss in detail the shift dependence on pump-burst duration, power, and wavelength.

3.3.1. Characterization of the light-induced frequency shift

The results on the dynamics of the optical tuning are analyzed in Figure 3.2, where the frequency shifts of individual molecules in the two host−guest systems are displayed (Figure 3.2.a,b for DBT:Ac and Figure 3.2.c for DBT:DBN). The experimental data represent the ZPL central frequency as a function of the cumulative pump exposure time and are extracted from the temporal map of the probe excitation spectrum *via* Lorentzian

fits. As the pictured data suggest, in each observed case the frequency shift slows down for long exposure times, with a characteristic time that typically varies among emitters and is, on average, different in the investigated matrix hosts. In general, such behavior can be fairly well described as a power-law function of time28 (dashed red lines in the figure are fits to the experimental data):

$$\nu(t) = \nu(0) + \beta(P)(t/t_0)^\alpha \tag{3.1}$$

Where ν is the molecule's ZPL central frequency, $\nu(0)$ its initial value, t the cumulative pump-exposure time, $t_0 = 1$ s the time normalization constant, α the power exponent, and the parameter $\beta(P)$ describes the extent of the frequency shift that can be achieved in a given exposure time. The specific dynamic parameters for the molecule's ZPL can vary among the two host matrices and even between different molecules within the same sample. This might be due to local differences in DBT concentration/orientation and to local crystalline impurities.
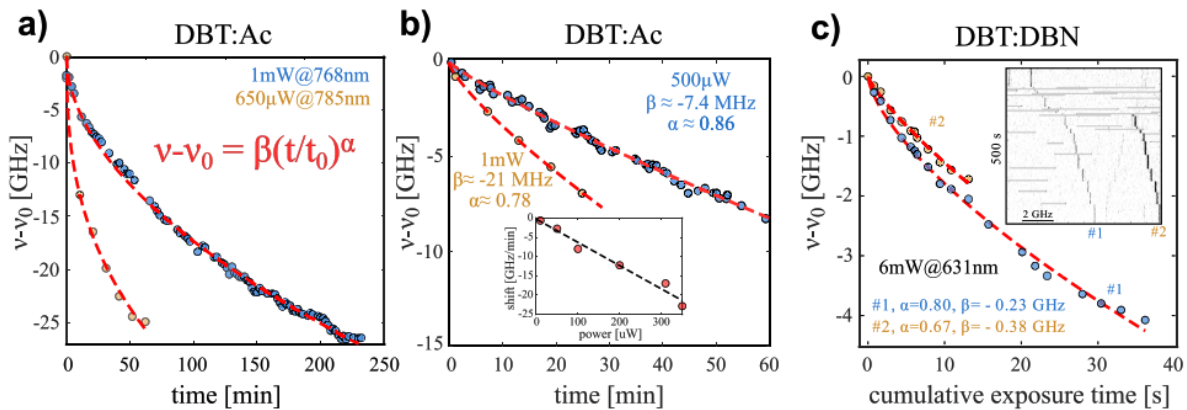

Figure 3.2: Dependence of the laser-induced shift on the exposure time and pump power for DBT:Ac (a, b) and DBT:DBN (c). The data points are the ZPL resonant frequencies obtained from a Lorentzian fit to the real-time excitation spectra, while the red dashed lines are power-law fits to the data. (a) Spectral shifts for pump laser frequency around the $0-1$ transition (blue points) and tuned $10\,GHz$ below ν_0 (yellow points) are compared. (b) Spectral shift dynamics for a DBT emitter pumped with different laser power. Inset: Spectral shifts of a second molecule subject to several 2 min long bursts at increasing power show a linear dependence on pump beam power. (c) Spectral shift as a function of cumulative exposure time for two DBT emitters (indicated as #1 and #2) in DBN. Inset: Frequency scans shown in real time (one line scan is 5 s). The gray horizontal lines indicate intermittent, short pump laser exposures (0.5 to 3 s).

Interestingly, no clear difference is observed in the induced shifts upon variation of the pump laser wavelength over a range of several nanometers (see also the SI). This suggests that the shift phenomenon can only be partially due to photon absorption by the shifting molecule. Indeed, this eventuality is ruled out by tuning the pump laser to the red of the molecule's ZPL, where no excited states exist. Figure 3.2.a shows in yellow dots the results of such an experiment, performed interrupting the pump illumination at regular intervals for about 1 h time. Despite a pump detuning of $10\,GHz$, a large frequency shift of $> 20\,GHz$ is observed. Every DBT emitter conversely shows a clear dependence on the pump-laser power. Specifically, when comparing shifts induced in the very same

molecule, the parameter β is strictly increasing with the pump laser power and, for short enough illumination times, has a linear dependence. In Figure 3.2.b two frequency shifts operated on the same molecule, exposed to different values of the pump laser power, are compared. In particular, for the higher power the ZPL is probed during brief interruptions of the pump illumination every few minutes, since a real-time measurement is precluded by the increased background fluorescence. In the inset of Figure 3.2.b, a collection of data is displayed for a molecule in a different nanocrystal, which exhibits considerably larger frequency shifts and enables a characterization for low pump power values. In this case the experimental data represent the overall frequency shifts observed after single illumination bursts of 2 min each with increasing pump power, illustrating the linear behavior of $\beta(P)$ for short illumination time. This result rules out the possibility of the direct two-photon-induced photoionization of the matrix, which would have a quadratic power dependence.

Qualitatively similar trends are reported for DBT:DBN in Figure 3.2.c, where two DBT emitters in the same DBN crystal are simultaneously shifted using a sequence of short, high-power, laser bursts. The burst duration varies between 0.5 and 3 s with a constant laser power of 6 mW. While one of the molecules undergoes photobleaching or large spectral jump during the process, the other accumulates a total shift of $4\ GHz$ in less than $40\ s$ of cumulative excitation. More results on intermolecular differences in the DBT:DBN system are available in the SI.

We note that for the results presented in Figure 3.2.=a−c, the modest fluctuations overlapping with the frequency shift in the emission can be related to spectral wandering, which is enhanced at the high power levels reached during pump exposure.

3.3.2. Tuning molecules into resonance

The advantages of the all-optical frequency tuning presented here are its spatial resolution and the flexibility of operation. Indeed, the effect is directly activated on the emitting sample with no need for additional nanofabrication steps (e.g., lithography or etching in order to define the electrodes), and being confined to the confocal beam volume, it enables spatial resolution at the micron level. On the other side, once doped with single-molecule concentration, homogeneously deposited on the substrate via drop-casting and desiccation, [27] or even integrated in nanophotonic structures, [15] DBT:Ac nanocrystals allow for spatial isolation of individual molecules, which can thus be selectively tuned by laser focusing. This is shown in Figure 3.3, where the ZPL peaks of five nearby molecules, each contained in a different nanocrystal (data of different color), are probed at regular time intervals while exposing only one of the molecules to 2 min long laser pulses with increasing power. The corresponding molecule (blue in the figure) undergoes a large shift of about $100\ GHz$ (~ 0.20 nm, corresponding to about a fifth of the inhomogeneous broadening and 2000 times the natural line width), whereas the transition frequency of others is not affected. In the inset, a wide-field fluorescence map shows the location of the respective nanocrystals, labeled with the same color code as in the main figure. Their

relative distance amounts to approximately $10\,\mu m$ and is determined by the NCX suspension density before deposition. We note in passing that the limit to the spatial resolution of this approach has not been touched here and is likely determined by the specific charge migration mechanism in the sample.
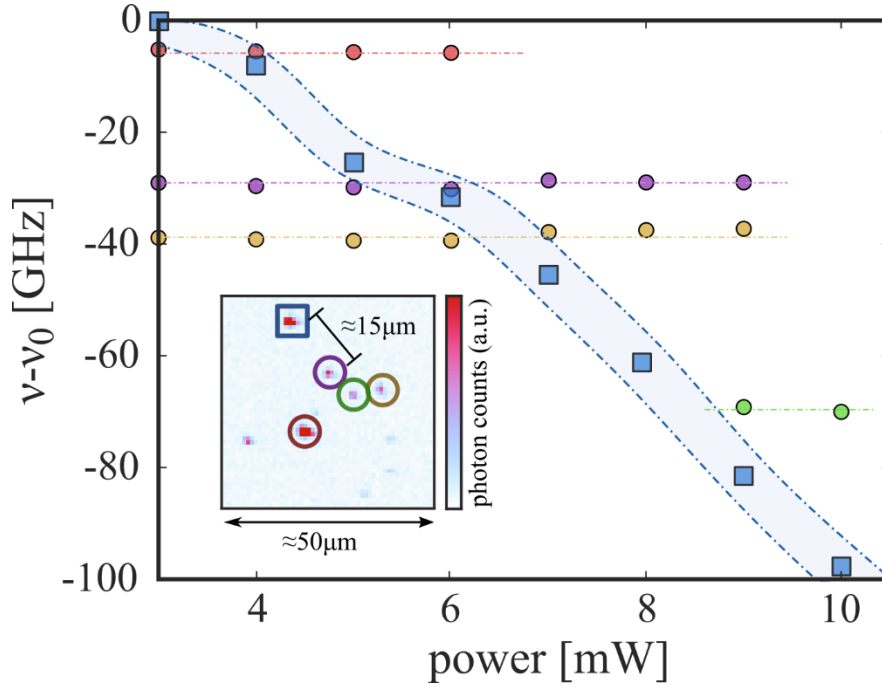

Figure 3.3: Localized frequency tuning. The central frequency of the ZPL is reported for several molecules as a function of the pump laser power, which only affects one of them (blue squares). The spatial distribution of the doped nanocrystals is given in the inset fluorescence map, revealing that as-close-as-15 μm molecules are completely unaffected by the manipulation.

Then we show the scalability of the proposed tuning approach, by shifting independently in a controlled way the ZPL of up to five close-by molecules, which are all brought on resonance within twice their line width. As in the case of the measurements shown in Figure 3.3, the emitters are embedded in different nanocrystals. Moreover their emission line widths, shown with the dashed lines in Figure 3.4, are originally well-separated by $20\,GHz$. The nanocrystals are addressed by the confocal pump-beam spot one after the other, independently, in order to shift their initial transition frequencies to a common targeted value. The latter, because of the dominant quadratic Stark effect in the Ac-matrix, is necessarily chosen as $\nu_0 \leq \nu_i$, where i labels the molecules' original emission frequencies. Based on previous calibration, the magnitude of the shift is adjusted by controlling the radiation dose (illumination power per exposure time). In general, the time required to shift the emission to a target frequency, which depends on the overall shift width, can be brought down to few minutes by playing on the pump laser power, as described in Figure 3.2.b. This is sufficiently quick to enable successive corrections for possible frequency deviations and hence preserve the target position for the time required to perform an experiment. The final excitation spectra are reported in Figure 3.4 using solid lines with shaded underlying areas in different colors, demonstrating fine-matching of five molecules, within about a two-line width range. Total shifts of up to about $20\,GHz$

can be estimated by comparing the final values with the initial ones. In Figure 3.4.b, the relative wide-field fluorescence map is reported, showing the simultaneous excitation of all molecules by means of the probe beam centered at the targeted frequency ν_0. Correspondingly, the bright spots highlight the spatial configuration of the synchronized nanocrystals. We finally observe that similar results have been obtained on different substrates, with nanocrystals deposited either on gold (SI), with a total shift of more than $20\,GHz$, or on sapphire (Figure 3.4). In particular, the current residual detuning of about two-line widths reported for five molecules and a line width for two molecules only depends on the spectral fluctuations arising during the pump-exposure process. Several mitigation techniques could be suitably implemented in the future to monitor and control the mutual frequency overlap of the emitters' ensemble, including an additional electrical bias to stabilize local charges.
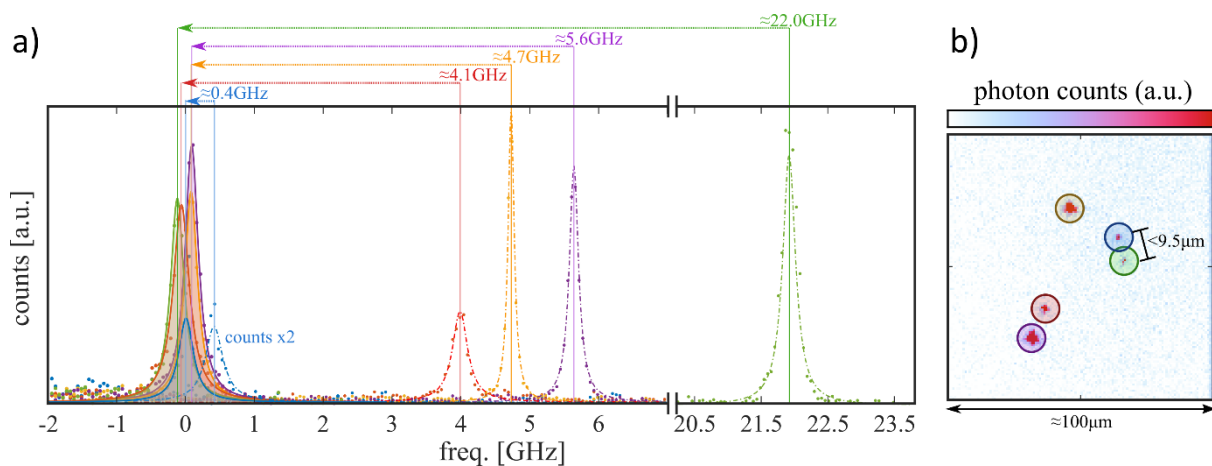

Figure 3.4: Frequency matching of five distinct molecules can be observed in the excitation spectra displayed in (a) as solid lines with underlying shaded areas. This exceptional condition is the result of a set of individual shifting applied to the original configuration, corresponding to the spectra reported as dashed dotted color lines. (b) Fluorescence map showing the simultaneous excitation of all nanocrystals when the probe is centered around ν_0 and applied in wide-field configuration.

The demonstrated results clearly show together several advantages of the proposed tuning approach: scalability, flexibility in the choice of substrate, high spectral and spatial resolution, and broad tunability range compared to the system's inhomogeneous broadening. We believe such characteristics will be crucial for the coupling of multiple emitters together in linear optical computing or simulation experiments and for the integration of molecules into resonant photonic structures.

3.3.3. Photoionization model of the laser-induced charge separation

In this section we propose a possible mechanism for our hypothesis of the laser-induced charge separation through photoionization of DBT molecules. We postulate a cascade photoionization mechanism for the buildup of the local electric field, *via* formation of long-lived charge-separated states.
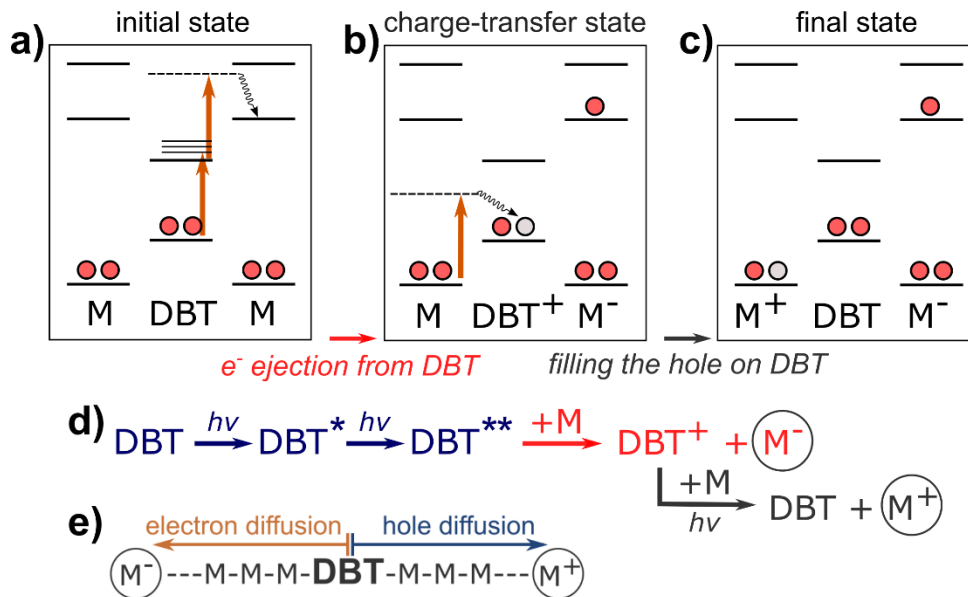
Figure 3.5: Proposed mechanism of the laser-induced charge generation. (a–c) Electronic energy diagrams describing (a) the initial electronic state and local excitation of DBT (red arrows), followed by electron ejection to the matrix (wavy line), (b) charge-transfer state and filling the hole on DBT, and (c) resulting final state of the system. Transitions induced by a single photon are shown with red arrows, virtual states are indicated by broken lines, and nonradiative CT transitions are indicated by wavy lines. Red and gray circles designate electrons and holes, respectively. M = matrix molecule (DBN or Ac). (d) Photoionization scheme that represents the path sketched in panels (a)–(c). $h\nu$ = energy of a pump-beam photon; excited electronic states are represented with the star symbol. (e) The resulting charge carriers (M^+ and M^-) diffuse further into the charge-separated states under the illumination of the pump beam.

The proposed model is based on the following assumptions:

1. The laser-induced excitation of DBT molecules leads to their photoionization by electron ejection.

2. The process results in long-lived charge-separated states in the matrix. The initially excited DBT molecules may be regenerated to their neutral state.

3. The photoionization of DBT results in mobile charge carriers (electrons and holes, with different mobilities) and their transport to larger distances (on the order of tens of nanometers at least).

4. The charge separation and trapping of electrons and holes result in the buildup of a static electric field which shifts DBT's ZPLs through a Stark effect (quadratic for DBT:Ac and linear for DBT:DBN).

The laser-induced charge separation mechanism is outlined in Figure 3.5. The initial step of the charge generation process is the photoionization of DBT molecules by intense pump light (Figure 3.5.a). This process requires at least two laser photons: a first DBT excitation with one pump photon (1.61 eV for DBT:Ac or 1.96 eV for DBT:DBN) to its first excited electronic state (S1), followed by a further excitation with a second pump photon (red arrows in Figure 3.5.a). Such a highly excited electronic state of DBT can

presumably eject an electron to the matrix (M) and give birth to a charge-separated state (DBT^+/M^-). Finally, the hole left on the DBT molecule may be transferred to the matrix through a single-photon excitation (Figure 3.5.b), yielding back a neutral DBT molecule and a matrix cation (M^+) (Figure 3.5.c). Figure 3.5.d summarizes the proposed photoionization cascade. However, while this is one of the most likely mechanisms, we note that other possible channels of light absorption and photoionization are also possible. The presence of dimers or clusters of DBT molecules, for instance, as well as other impurities, can red-shift the absorption spectrum by up to several thousands of cm^{-1}. This can explain the occurrence of the photoionization phenomenon for a broader range of pump frequencies. Notably, we observed that the spectral shifts in both DBT:Ac and DBT:DBN can be induced by using a pump beam at 795 nm, which is outside the inhomogeneous broadening of the studied systems (200 and 650 cm^{-1} below the ZPL, respectively).

The migration of the induced charge carriers is possibly further activated by the pump beam, leading to charge diffusion and to charge-separated states (M^+ and M^-) far enough from each other so that the recombination probability becomes negligible (see Figure 3.5.e). It is important to realize that, if the initial DBT molecule is regenerated to its neutral state, the process can be repeated many times. In effect, each DBT molecule may give rise to a macroscopic charge distribution in its environment. The resulting charge density buildup shifts ZPLs of DBT probe molecules by the Stark effect.

Our photoionization scheme is inspired by earlier models of photoconductivity in organic solids. The inclusion of larger PAH impurities into an anthracene crystal, such as tetracene, significantly reduces the activation energy for the charge-carrier transport. [29–31] Likewise, the proposed charge separation mechanism is the key to the photorefractive effect in multicomponent photorefractive materials doped with optically active organic molecules.[32]

The suggested model is consistent with the continuous shift of the molecule's ZPL resonance, as well as with its narrow line, which rules out any heating-induced rearrangements. The Stark shift associated with a net field buildup well captures a shift that can have opposite signs for DBT:DBN, while is only toward longer wavelengths for DBT:Ac. Further details on the consistency between the model and the experimental observations are provided in the SI.

Finally, simple quantum chemistry calculations have been performed, which qualitatively support our photoionization model. All three steps presented in Figure 3.5 are found to be energetically feasible according to time-dependent density functional theory (TDDFT/B3LYP). For the details of the calculations, the reader is referred to the SI. Beyond the first electronic excitation, several higher electronic states of DBT are found above 3.0 eV, suggesting that excitation of DBT with two red photons is likely to happen under experimental conditions of strong illumination. According to the calculations, the following step of electron transfer to the matrix could be phonon-assisted for DBT in Ac,

while a direct excitation of the charge-transfer (CT) state may operate as well for the DBT:DBN system. The formation of the CT excitations on the neighboring molecular sites is considered important for the transport properties of photoexcited organic materials. [33] Nevertheless, due to their short lifetimes, [34,35] the CT states cannot explain the buildup of the stable electric field, which persists for long time after the excitation. These states can be rather considered as the precursors for the photoinduced formation of free electrons and holes, which are separated to larger distances by the pump beam. The transport of charges is further supported by the presence of many host molecules in the crystals, which results in the formation of a quasi-band structure of CT-type electronic states (see the SI).[36] Concerning the regeneration of neutral DBT molecules, several CT transitions are found from Ac to DBT$^+$ within the energy range of our excitation (1.6 eV). Lastly, the further transfer of charge carriers through the matrix to distances larger than several unit cells is assumed to take place through interaction of charged species with red light. Indeed, we find that Ac^+, Ac^-, and DBT$^+$ can all absorb red photons, which is in line with other theoretical results. [37]

3.4. Conclusion

We have demonstrated optically induced tuning of light emission from single DBT molecules in two different types of molecular crystals that are of interest for molecule-based integrated quantum devices. Tuning by up to 0.2 nm ($\sim 1/5$ of the inhomogeneous broadening) has been observed, persisting for a macroscopic time (several hours), which allows the successive manipulation of several independent molecules. Because of the predictability of the frequency shift, we were able to tune five independent molecules on the same ZPL emission wavelength within twice their line width. Such fine control of an emitter's transition frequency, together with the achievable tuning range, might empower the presented technique in any context involving molecular emitters coupled to resonating photonic structures and/or multiple sources emitting at the same wavelength, such as in optical quantum computation, simulation, and communication.

We emphasize the potential applicability of our methodology to a broad range of host/guest molecular systems. Studying light-induced charge dynamics with single-molecule sensitivity could shed light on the microscopic mechanisms behind photoconductivity in organic solids and motivates the exploitation of single molecules in quantum technologies and molecular electronics. Many possibilities to further fine-tune and manipulate optical transitions of molecules can be envisaged in this context. Finally, tuning light emission of many single emitters by using this simple optical approach may become an important step in integrating single emitters into robust quantum protocols based on molecules.

3.5. Supporting Information

3.5.1. Measurements of DBT:Ac nanocrystals

Shift dependence of power and pump laser wavelength
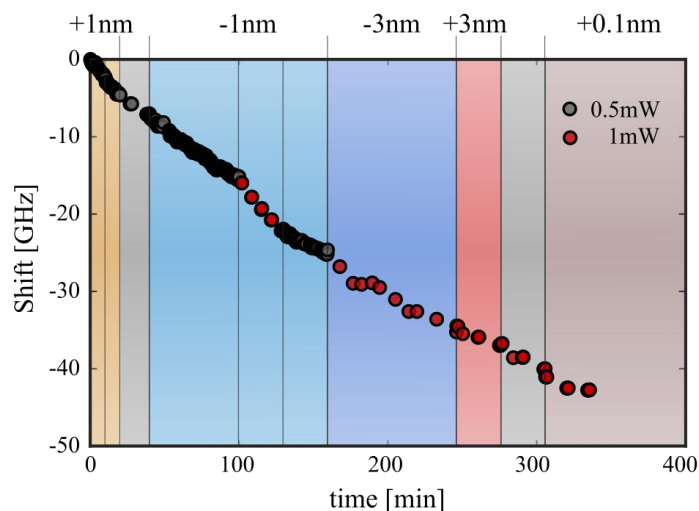

Figure S3.1: 0-0-ZPL transition shift induced on the same single molecule by a succession of "pump" laser bursts with different characteristics (wavelength and illumination power). The data-points are the ZPL resonant frequencies obtained from a Lorentzian fit to the excitation spectra. Data-points colors refer to the pump power value, whereas the temporal color-bands indicate the pump wavelength with respect to the most efficient excitation rate of the 0-1 transition, labeled in gray and corresponding to the pump at 767.8nm.

In Figure S3.1 the entire dynamics of the ZPL-transition frequency shift for an individual DBT molecule in an Ac-nanocrystal is reconstructed by monitoring its position after several consecutive burst exposures, operated with different parameters (illumination power and wavelength). The temporal colored bands indicate the pump wavelength value, according to the labeling on the right. Furthermore, colors of the dotted data refer to the two employed pump powers, one double (red) the other (black). This latter parameter change can be used as term of comparison: while the induced-shift dynamics is clearly dependent on the pump power (see also Figure 3.2.a in the main text), it is not visibly sensitive to wavelength. Consequently, we can state that the photochemistry process responsible for the charge separation and the Stark shift does not result from excitation of the DBT molecule under single-molecule investigation. Indeed, the spectral band explored in the measurements reported in Figure S3.1 corresponds to very different pumping efficiencies for a given illumination power. By comparison with a reference excitation spectroscopy of the 0-1 transition obtained for a different molecule (Figure S3.2), the excitation wavelengths labelled in gray in Figure S3.1 correspond to the strong peak at 764.7 nm, hence to the maximum excitation efficiency. The wavelength labelled in orange is instead associated to the plateau between the two resonance peaks, hence to an excitation efficiency reduced by more than one order of magnitude, while for 3 nm on the red (red band), we are close to the secondary resonance. Moreover, on the blue of the main peak it is established that no relevant resonances are present within 7 nm shift [S2] (not shown).
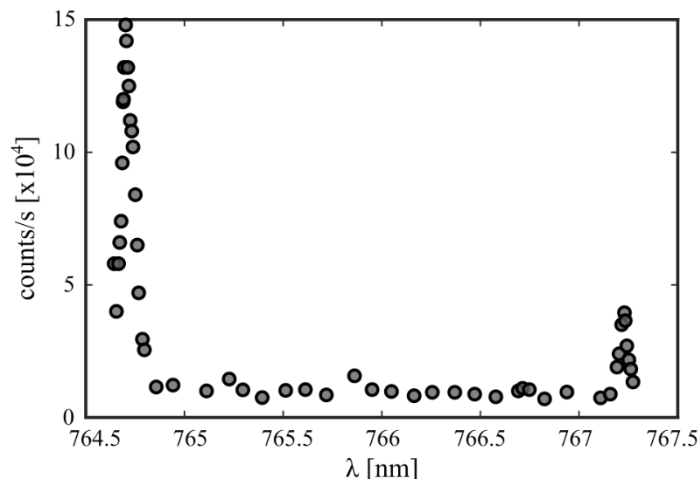
Figure S3.2: Excitation spectroscopy performed with the "pump" laser around the 01-ZPL transition: recording the spectrally integrated fluorescence intensity gives access to the pumping efficiency as a function of illumination wavelength. The reported spectrum is not measured for the same molecule of Figure S3.1, and in particular the main excitation peak in this case was shifted by around 3 nm to the blue with respect to the molecule of Figure S3.1. However, we have found evidence that the level scheme is almost rigidly shifted by the inhomogeneous broadening. Our findings are in substantial agreement with ref.[S2].

Despite this big variation on pumping efficiency, the laser-induced shift recorded in Figure S3.1 is not correspondingly affected by the difference in the excitation efficiency of the DBT molecule under investigation, as a function of the pump laser frequency. This is a relevant indication that the light-induced shift does not depend strongly on the target molecule's ZPL-transition.

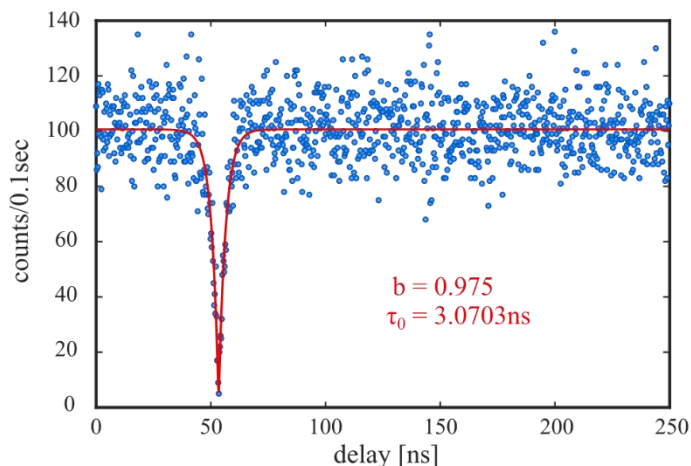**Measurement of the photon statistics: single photon purity**

Figure S3.3: Anti-bunching measurement for fluorescence collected from an individual DBT:Ac nanocrystal under illumination with "pump" laser at 767 nm, evaluated as a histogram of the differential arrival times of the photons on two avalanche photodiodes in a Hanbury-Brown and Twiss configuration. The second-order autocorrelation function at zero delay is inferred by the best fit (red line) to the experimental data (blue dots), yielding $g^{(2)}(0)$=1-b=0.03±0.03. In particular, the fit function is $g^{(2)}(t) = A(1 - be^{-|t-t_0|/\tau})$, with A normalization factor, b anti-bunching dip depth, t_0 a time delay and $1/\tau$ accounting for the excitation and spontaneous emission rate.

In Figure S3.3 we show a representative example of anti-bunching measurements of an individual DBT:Ac nanocrystal. The data points are recorded under off-resonant excitation (767 nm). The second-order autocorrelation function at zero delay inferred by the fit to the experimental data yields $g^{(2)}(0)=1-b=0.03\pm0.03$, which proves the high purity of the single-photon emission. This result is not in contradiction with the measurements reported in the main text (Figure 2), where we see a background comparable to the signal intensity. Indeed, shift measurements are performed with a strong illumination power (exciding by more than one order of magnitude the saturation level), which is able to excite other, more weakly coupled molecules. The latter are molecules without narrow lines, or with narrow lines at different wavelengths and/or spatially close to the one under investigation. With respect to the last "background source", a relevant gain is obtained also thanks to the spatial selection introduced by fiber-coupling.

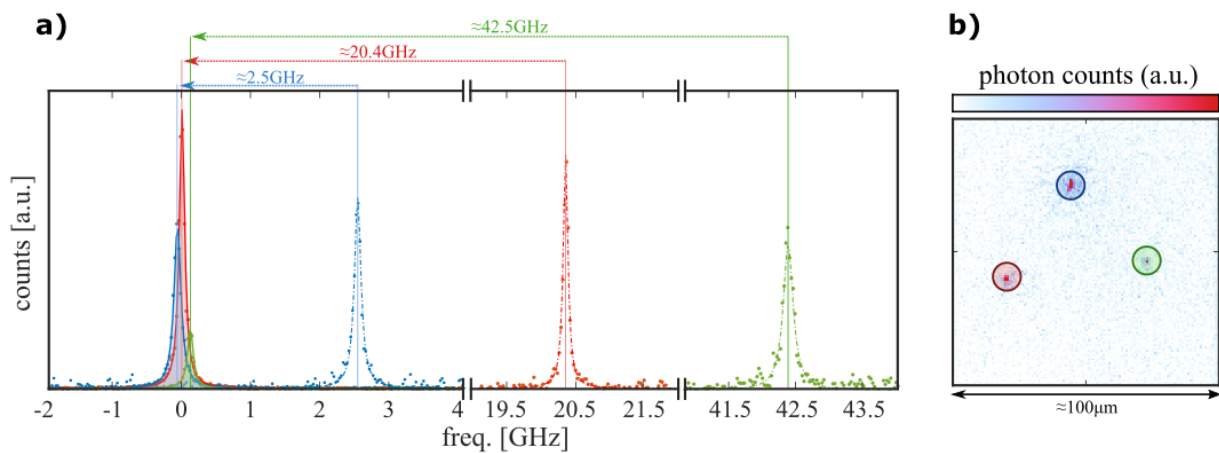**Independence on the sample substrate**

Figure S3.4: Frequency matching of three distinct molecules deposited on a gold substrate can be observed in the excitation spectra displayed in a) as solid lines with underlying shaded areas. This condition is the result of a set of individual shifting applied to the original configuration, corresponding to the spectra reported as dashed dotted color lines. b) fluorescence map showing the simultaneous excitation of all nanocrystals when the probe is centered around ν_0 and applied in wide-field configuration.

As mentioned in the main text, the shift phenomenon is independent on the substrate on which the NCX are deposited. Indeed, in Figure. S3.4 we report the result of an experiment in which three different DBT:Ac emitters, deposited on a gold substrate, have been tuned to the same reference frequency. The experiment is conceptually identical to the one reported in Figure 3.4 of the main text. However, in the case of DBT:Ac on gold, the accuracy can be slightly increased because of the generally stronger emission that one can get from emitters deposited on gold substrate with respect to glass substrate.

3.5.2. Measurements of DBT:DBN single crystals

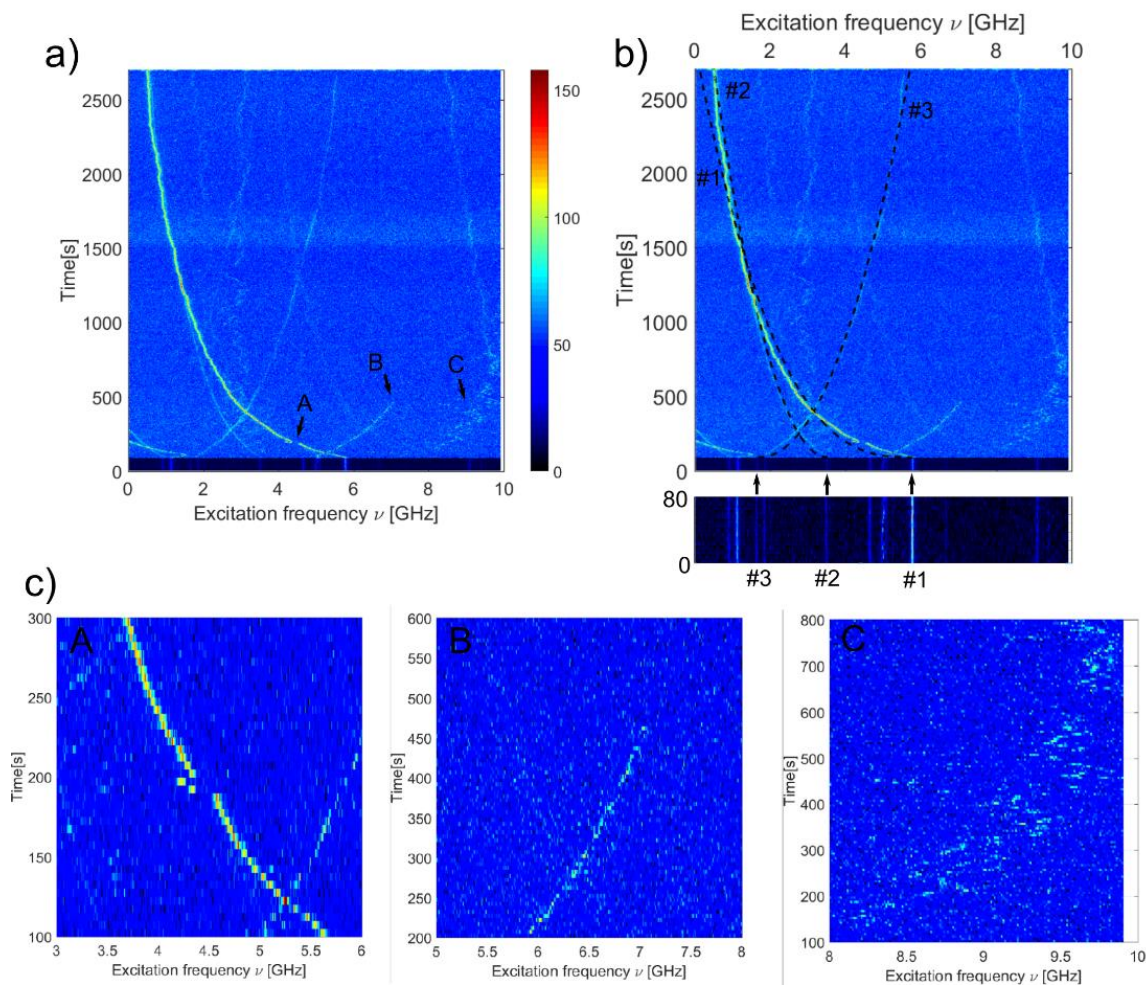**Single-molecule trajectories and inter-molecular heterogeneity**

Figure S3.5: a) Single-molecule fluorescence excitation spectrum of DBT molecules in 2,3-DBN recorded in real time during exposure to a pump beam (631 nm, 45 µW). Several ZPLs are visible showing different response to the pump beam. Highlighted events A-C are shown in (c). The dark blue background at the bottom indicates line scans without the pump beam. The probe beam was continuously scanned at 756.7 nm (0.7 µW). Color bar: counts per 5 ms. b) Power law fits for three molecules, indicated with arrows; molecule #1 (α=0.36, B=-340 MHz), molecule #2 (α=0.49, B=-60 MHz), and molecule #3 (α=0.47, B=100 MHz). The coefficients α and B are as in eq. (1) of the main text. Note that molecule #1 has the largest shift, but also the largest departure from the power law fit. c) Typical examples of a smaller spectral jump possibly influenced by a nearby charge diffusion (A), large spectral jump or photobleaching event (B) and large and fast spectral diffusion with fast random jumps (C).

DBT:DBN single crystals are prepared by a co-sublimation method, using zone-refined DBN. This method is considered to produce molecular crystals of highest quality and purity. Furthermore, using these crystals with relatively high concentration of well-embedded DBT molecules, we can locally sense charging events, charge migration and fluctuations in electric field buildup. As each molecule is embedded in a slightly different environment, the response of individual molecules may differ. Figure S3.5 illustrates this on a set of several molecules. Apart from fairly stable trajectories in molecules #1, #2, and #3, one can discern other types of trajectories and local behaviors. For example, molecule #1 exhibits a small spectral jump

(labelled as A in Figure S3.5.c) for ~ 10 s, which is likely an evidence of a nearby charging event. Event (B) highlights a molecule that suddenly photobleaches or undergoes a large spectral jump out of the frequency scan window (10 GHz). Trajectory (C) is from a spectrally unstable molecule that is seeing more frequent local perturbations due to local charge dynamics.

Power law behavior of individual trajectories

Figure S3.5.b shows power law fits to three long trajectories presented in Figure S3.5.a. As can be seen, all molecules do not display the same electric field change, and their trajectories are quantitatively different. Furthermore, power law functions cannot fully describe the behavior of all individual molecules, but it is a fairly good approximation on larger timescales of up to 1 h. For example, molecule #1 in Figure S3.5.b shows the largest response to the pump beam, but its behavior is not well-fitted by a power law. On the other hand, molecules #2 and #3 show a fairly good match with a power law behavior and their fitting parameters are very similar, even for longer timescales.
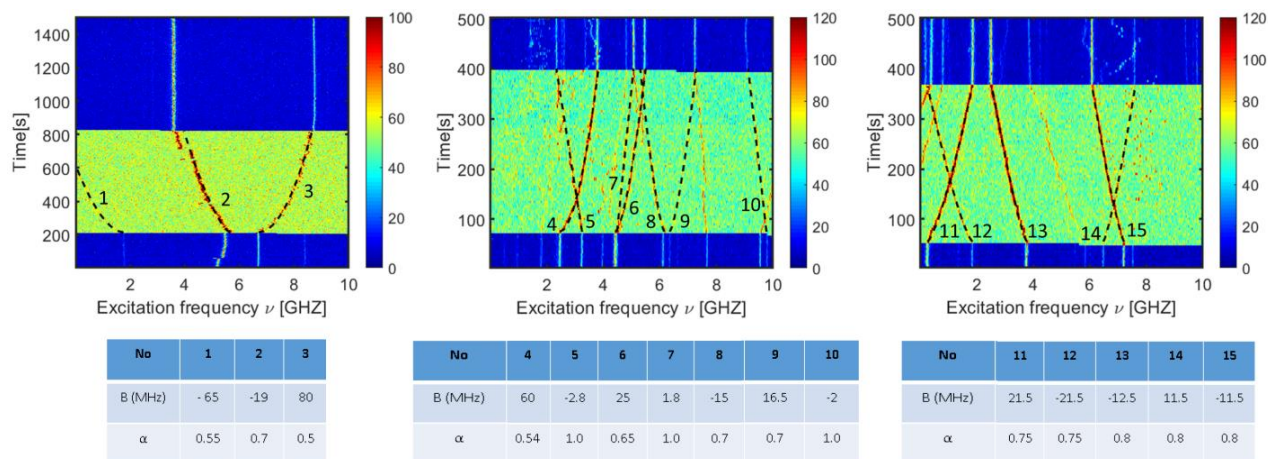

No	1	2	3
B (MHz)	- 65	-19	80
α	0.55	0.7	0.5

No	4	5	6	7	8	9	10
B (MHz)	60	-2.8	25	1.8	-15	16.5	-2
α	0.54	1.0	0.65	1.0	0.7	0.7	1.0

No	11	12	13	14	15
B (MHz)	21.5	-21.5	-12.5	11.5	-11.5
α	0.75	0.75	0.8	0.8	0.8

Figure S3.6: Examples of 15 single-molecule trajectories, recorded at different points on a DBT:DBN crystal. The trajectories are fitted with a power law equation, $\nu = \nu 0 + B \cdot (t/t_0)^\alpha$, where $t_0 = 1$ s. The table includes fitted parameters B (MHz) and α for all 15 molecules. The pump excitation power was in all experiments ~ 50 µW at 631 nm. Color bars: counts per 5 ms.

Despite the mentioned heterogeneities that are intrinsic to molecular systems perturbed with charging events at 1.2 K, we still find many molecules "well-behaving" in the pump beam. Figure S3.5 shows the examples of 15 single-molecule trajectories obtained on 3 different locations in a DBT:DBN crystal. All these trajectories (5 – 10 min long) are fitted well with a simple power-law equation. What is interesting to note is that up to several molecules in each scan can be fitted with very similar parameters B and α (e.g. molecules 11-15 in scan 3, Figure S3.6), indicating that these DBT emitters experience very similar local electric fields. We find parameter α mostly having values between 0.5 – 1.0, where the lower α designates faster initial change in resonant frequency of a molecule and α = 1 means linear time dependence.

ZPLs of individual molecules do not drift or jump after the pump beam is switched off, as shown in Figure S3.7. In this example the ZPL was tuned with a fairly low power of the pump

beam (43 µW). As shown in Figure 3.2 the ZPL lines remain stable and can be shifted much faster with more intense (6 mW), shorter pump pulses (1 – 3 s). This holds for a large majority of single emitters and indicates that charge reconfiguration in the crystal upon pump illumination is almost instantaneous, but it does no longer affect the frequency of the optical transition after the pump beam has been switched off. The latter observation indicates long recombination times and large electron-hole separations in the sample.
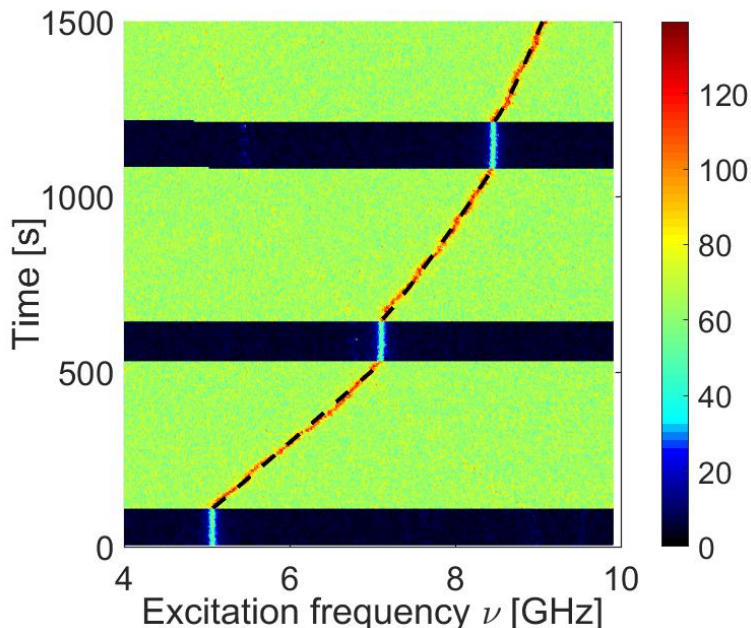

Figure S3.7: Start-stop experiment with alternating pump excitation (on/off), for DBT in 2,3-DBN. The pump beam excitation was 43 µW at 631 nm, whereas the probe beam (0,7 µW) was continuously scanned at 756.7 nm. Color bar: counts per 5 ms. Dashed lines represent power law fits to the data, with B = 5.2 MHz, and α_1=0.99 (bottom fit), α_2=0.92 (middle fit), α_3=0.84 (top fit).

Spectral shift power dependence in DBT:DBN

We have tested the behavior of individual emitters to increasing illumination powers of the pump beam. Figure S3.8 illustrates behavior of two emitters (#1 and #2) at three different powers, normalized to the dose of radiation. At 47 µW of pump illumination, the rate of shift change decays in time due to the power law behavior. Increasing of the pump power leads to further increase of spectral shifts and has close-to-linear power dependence. i.e., similar power-law trend is present when the shifts are rescaled to the dose of the pump beam.

Background fluorescence

Background fluorescence in both DBT:Ac and DBT:DBN originates from fluorescent molecules that are excited with the pump beam. In the latter case, the contribution is largely due to the non-resonantly excited background molecules. The measured signal has close to linear power dependence (Figure S3.9) indicating that we do not reach saturation of background signal at high excitation powers (above 1 mW).
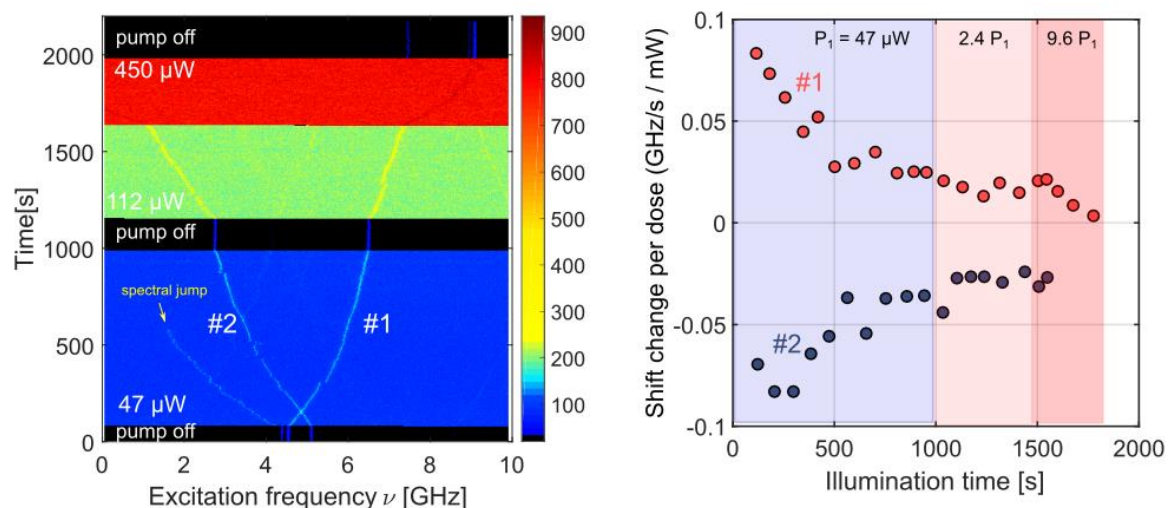
Figure S3.8: Left: Single-molecule fluorescence excitation spectrum of DBT molecules in 2,3-DBN recorded in real time with different pump beam excitation powers at 631 nm (47 µW, 112 µW, and 450 µW). Two stable ZPLs (#1 and #2) are visible showing fairly similar response to the pump beam. The black background in the image indicates line scans without the pump beam. The probe beam was continuously scanned at 756.7 nm (0.7 µW). Color bar: counts per 5 ms. Right: Shift changes for molecules #1 and #2 shown in the left image, plotted in real time. The color-coded zones denote regions of different pump power. The spectral jump indicated with a yellow arrow may be a signature of a discrete ionization or trapping event.
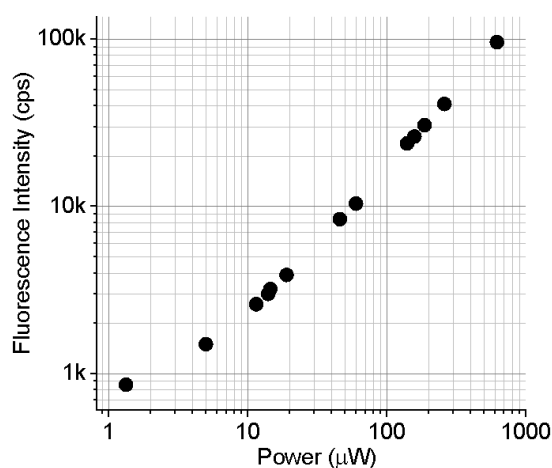
Figure S3.9: Fluorescence background signal change with excitation power of the pump beam at 631 nm. The background signal originates from many excited DBT molecules in 2,3-DBN single crystal.

We also observed that spectral shifts can be controlled by changing the polarization of the pump beam, affecting in this way the amount of excited DBT molecules (Figure. S3.10). The largest spectral shifts were obtained for the maximum of fluorescence background signal, proving that larger number of excited DBT molecules leads to greater charge generation and, consequently, larger spectral shifts.

Figure S3.10: Left: trajectories of two DBT molecules (#1 and #2) in DBN, whereby the polarization of the pump beam is varied with a λ/2 wave plate. The polarization state of the pump beam was adjusted in such a way that the background signal alternated betw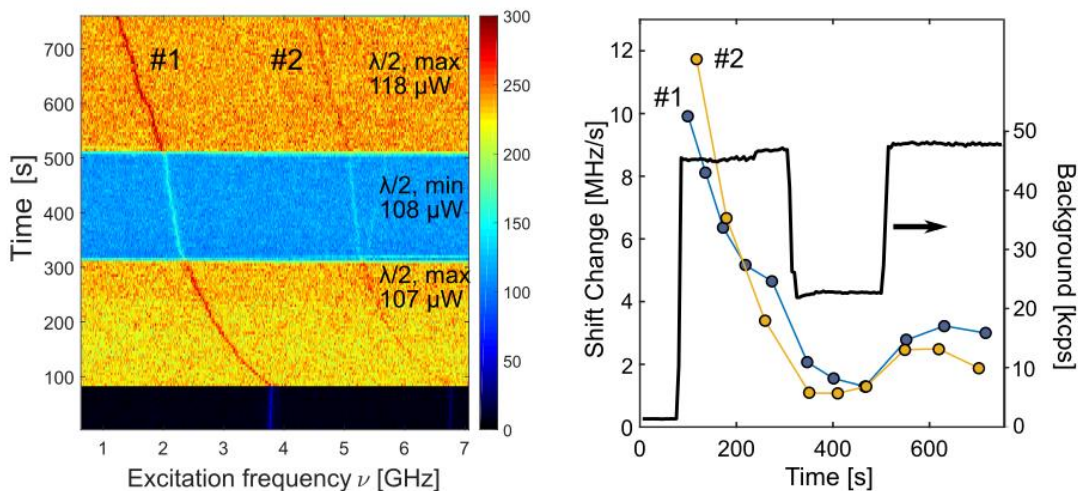een maximum (~47 kcps) and minimum (~22 kcps). To excite a larger number of molecules, the pump and the probe beam were previously circularly polarized with a λ/4 wave plate. Color bar: counts per 5 ms. Right: the average change of the spectral shifts in time for molecules #1 (blue circles) and #2 (red circles).

Dibenzoterrylene in polycrystalline naphthalene
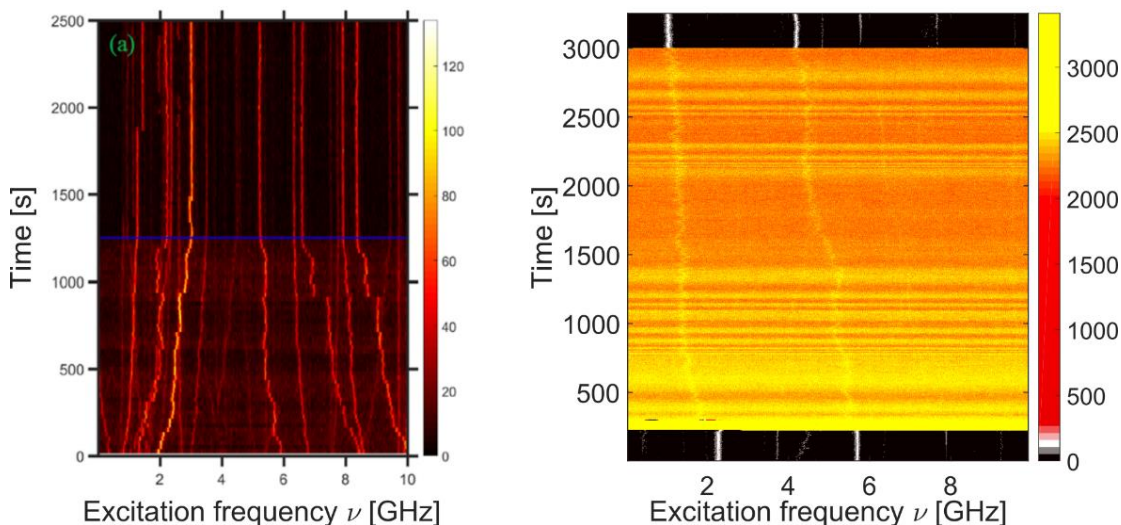
Figure S3.11: Tunable spectral shifts of DBT in polycrystalline naphthalene, with pump excitation at 570 nm (left) and 631 nm (right). Color scale counts per 5 ms.

Spectral shifts of DBT in polycrystalline naphthalene can be induced with a pump beam of broad excitation range. In this example (Figure S3.11), we have used a tunable pump laser at several wavelengths in a range of 570 – 635 nm. The ZPLs are photostable (no photobleaching or large spectral jumps) and the spectral shifts obtained are, on average, lower than in DBT:DBN and DBT:Ac systems, typically up to 1 GHz/mW per 1 hour of illumination. Spectral diffusion in this system is also more pronounced, with molecules changing the direction of their shifts in real time. The background signal has oscillating behavior (right panel). This pronounced background time-dependence is most likely due to the change in the

refractive index of a crystal, induced by migration of charges – an effect typically observed in photorefractive materials.

3.5.3. Quantum chemistry calculations

Quantum chemistry calculations were done in order to provide information about energies and character of electronically excited states in DBT/DBN and DBT/Ac crystalline systems. Performed calculations required big computer memory and were done by using the TDDFT/B3LYP method with 6-31G(d,p) or 3-21G bases. Theoretical calculations do not guarantee the same precision as the experimental data and thus should be treated with some caution. Calculations of electronic states in studied bimolecular systems (DBT:Ac and DBT:DBN) were performed for Ac and DBN molecules in their real crystal geometries. Embedding sites of DBT in both crystals were already optimized in our previous works. [S3, S4] Different substitution sites led to slightly different energies of the electronic states of DBT molecules embedded in DBN and Ac crystals.

Calculations on isolated molecules

Tables S1 provides useful information about excitation energies of isolated DBT, DBN, and Ac molecules. The calculated lowest energy transitions (ΔE) agree well with the experimental values. Electron affinities (EA) and ionization potentials (IP) of isolated molecules shown in Table S1 can be used as useful descriptors of electron and hole stabilities, as they determine the polarization energies of created charges in the studied systems. [S5] Based on the values of electron affinities and ionization potentials, the activation energy needed to put the system into a conducting state can be estimated. [S5, S6] According to this empirical description, energy levels of electrons and holes on DBT (i.e., DBT^- and DBT^+) will be in between the energy levels of charged host molecules (e.g., Ac^+ and Ac^-). DBT impurities will thus behave as traps for electrons and holes in both DBN and Ac. Therefore, the activation energy needed to drive the system into photoconducting state will decrease (from, e.g., 3.9 eV for pure anthracene crystal). This empirical interpretation of Karl and Silinsh is confirmed with our quantum chemistry calculations, as elaborated below in more details.

Table S3.1: Isolated DBT, DBN and Ac – excitation energies (ΔE), ionization potentials (IP) and electronic affinities (EA). TDDFT/B3LYP/6-31G(d,p) results.
Note that IP (DBT) < IP(Ac) < IP(DBN), and EA (DBT) > EA(Ac) >EA(DBN).

	ΔE [eV]	IP [eV]	EA [eV]
DBT	1.58	4.30	2.68
DBN	4.25	6.16	1.53
Ac	3.27	5.24	1.65

Energies of the excited electronic states of DBT

Energies and oscillator strengths for $S_1 \rightarrow S_i$ transitions of an isolated DBT molecule were calculated with the aid of the ab initio RHF CIS/3-21G (a convenient method is lacking in the frame of the TDDFT method included in Gaussian 09). It is well known that ab initio methods

give larger values for the transition energies, thus the results of the CIS/3-21G calculations included in Table S3.2 were scaled with factor 1.48. Such procedure led to quite good agreement between the $S_0 \rightarrow S_1$ transition energies calculated with the aid of both methods and describes well the experimental spectrum. An additional criterion for the sequence of states was their symmetry. Oscillator strengths for the $S_0 \rightarrow S_i$ transitions calculated by using the CIS/3-21G method were systematically bigger than the corresponding values obtained with the TDDFT/6-31G(d,p) method, but relations between different transitions are similar. Taking into account these observations, we note high oscillator strengths of the transitions $S_1(Au) \rightarrow S_4(Bg)$ and $S_1(Au) \rightarrow S_7(Ag)$, with the energies ~1.3 eV and ~1.5 eV, respectively. Our results are in agreement with the results of calculations described in the work of Sadeq et al.[S7] In conclusion, both states, $S_4(Bg)$ and $S_7(Ag)$, can be involved in the excitation from the $S_1(Au)$ state, as proposed in our photoionization model which includes CT states (see below).

Table 3.2: Energies of excited electronic states of DBT molecule and the oscillator strengths (f) for the $S_0 \rightarrow S_i$ [S8] and $S_1 \rightarrow S_i$ transitions.

| | | TDDFT/B3LYP/6-31G(d,p) | | | CIS/3-21G | | | |
| | | $S_0 \rightarrow S_i$ | | $S_1 \rightarrow S_i$ | $S_0 \rightarrow S_i$ | | $S_1 \rightarrow S_i$ | |
i	sym	ΔE [eV]	f	ΔE [eV]	ΔE [eV]	f	ΔE [eV]	f
1	AU	1.584	0.383		1.533	1.105		
2	BG	2.601	0.000	1.017	2.583	0.000	1.049	0.022
3	AG	2.703	0.000	1.119	2.937	0.000	1.404	0.054
4	BG	2.872	0.000	1.288	3.012	0.000	1.479	0.640
5	AU	2.994	0.006	1.410	3.441	0.022	1.908	0.000
6	BU	3.087	0.010	1.503	2.760	0.011	1.227	0.000
7	AG	3.131	0.000	1.547	3.077	0.000	1.544	1.140
8	AU	3.267	0.201	1.683	3.159	0.157	1.626	0.000
9	BG	3.339	0.000	1.755	3.343	0.000	1.810	0.381
10	BU	3.354	0.012	1.770	3.288	0.021	1.755	0.000
11	BU	3.504	0.060	1.920	3.474	0.838	1.941	0.000
12	BG	3.593	0.000	2.009	3.700	0.000	2.166	0.046
13	BG	3.800	0.000	2.216	3.893	0.000	2.360	0.014
14	BU	3.844	0.418	2.260	3.995	0.231	2.462	0.000

Calculations of locally excited (LE) and charge-transfer (CT) states

In this work, we make a distinction between two types of excited electronic states, which are characteristic for molecular solids and relevant for this work. The electronic excitation of a system with two or more molecules can lead to rearrangement of electronic charges between molecules, creating intermolecular electron transfers, or charge-transfer (CT) states. If such rearrangement of electron density happens intramolecularly, we talk about locally excited (LE) states. The electronic excited states may have also partially LE and partially CT character.

Electronic states and transitions of bimolecular DBT/DBN system

Table S3.3: TDDFT/B3LYP/3-21G results of energies and character of the electronic states in DBT/DBN system, calculated in the real crystal structure geometry of DBN. Red color in the energy levels diagram on the right indicates the contribution of CT character in the presented states. The states CT1 and CT3 are purely CT (DBT→DBN) states. The state CT2 has comparable contribution of the CT and LE characters. Electronic excitations S_1→CT2 and S_1→CT3, indicated by the red arrows, are supposed to contribute to the transfer of an electron from DBT to the nearby DBN molecule, leaving a hole on the DBT.

i	$\Delta E(S_0 \rightarrow S_i)$ [eV]	f	character of the dominant configuration of the electronic state
1	1.823	0.428	LE(DBT→DBT)
2	2.667	0.001	**CT1(DBT→DBN)**
3	2.671	0.002	LE(DBT→DBT)
4	2.778	0.002	LE(DBT→DBT)
5	2.843	0.004	LE(DBT→DBT)
6	2.955	0.001	BCT(DBN→DBT)
7	3.030	0.029	LE(DBT→DBT)
8	3.252	0.013	LE(DBT→DBT)
9	3.279	0.008	LE(DBT→DBT)
10	3.375	0.090	LE(DBT→DBT)
11	3.428	0.100	LE(DBT→DBT)
12	3.462	0.021	BCT(DBN→DBT)
13	3.541	0.083	LE(DBT→DBT)
14	3.553	0.030	LE(DBT→DBT)
15	3.618	0.013	**CT2(DBT→DBN)**
16	3.819	0.001	**CT3(DBT→DBN)**
17	3.842	0.024	LE(DBT→DBT)
18	3.938	0.149	LE(DBT→DBT)

The lowest-energy electronically excited state of the DBT/DBN system, S_1, is localized on the DBT component. A sequence of two excitations which would be in agreement with the excitation energies applied in the experiment (~ 2.0 eV), goes as follows:

1. $S_0 \rightarrow S_1$(DBT), energy ~1.8 eV , and next
2. S_1(DBT) $\rightarrow S_{15}$(CT2), S_{16}(CT3), S_{17}(LE), with excitation energy in range 1.8-1.9 eV.

Also, the nearby S_{14} and S_{18} states, attributed in Table S3 to LE states, have some contribution of CT character and thus may contribute to the electron transfer from DBT molecule to the surrounding DBN matrix. All these calculated transitions are within the excitation energy of the pump beam (~ 2 eV). High excitation powers are needed to excite a DBT molecule from the S_1 state to some higher electronic states with CT character, before the molecules relaxes back to the ground electronic state.

Electronically excited states of DBT:Ac system

Electronically excited states of DBT/Ac system were calculated for two molecules, DBT and Ac, as well as for a DBT molecule surrounded by 4 molecules of Ac, arranged in the crystal geometry, as shown in Figure S3.12. The results of calculations are collected in Table S3.4 and graphically presented in Figure S3.12. The results for isolated DBT and Ac are also shown in Figure S3.12 for comparison.
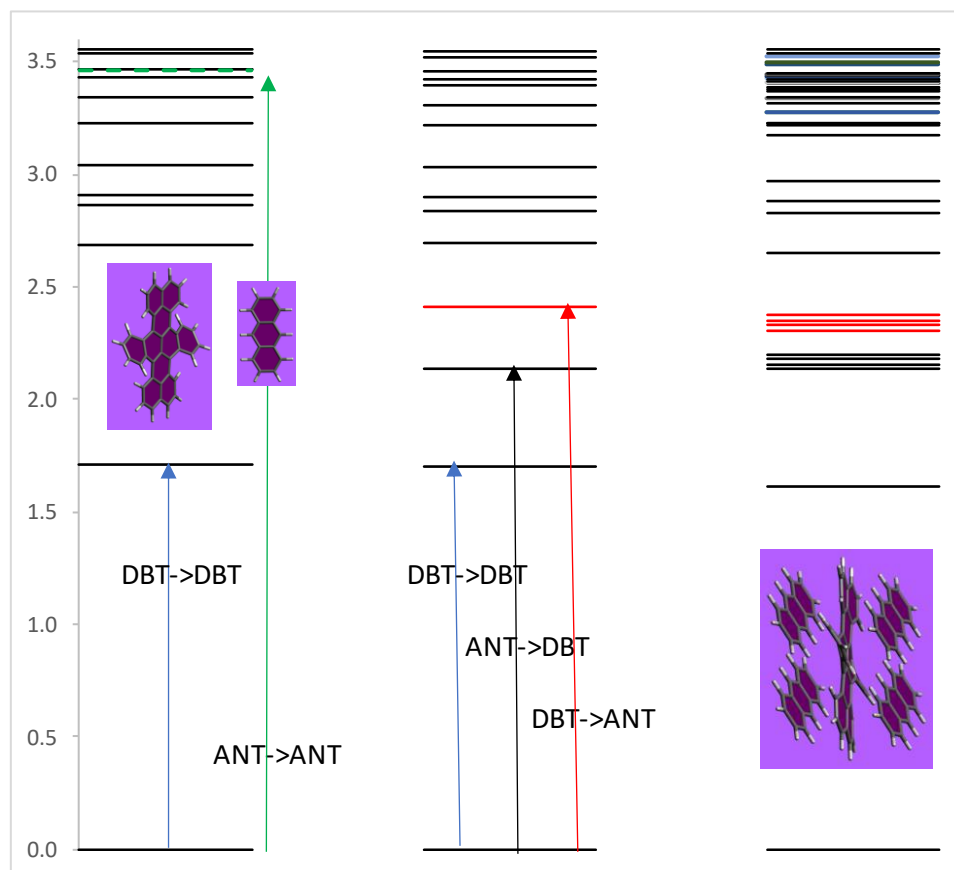

Figure S3.12: Diagrams of the electronic excited states of isolated DBT and Ac molecules (left), in the system composed of DBT molecule and one Ac molecule (center) and DBT surrounded by 4 molecules of Ac (right). Numerical data for DBT+4Ac are collected in Table S3.4.

Table S3.4: Energies and oscillator strengths of electronic transitions in the system DBT+4Ac molecules. Different colours were used to distinguish transitions with different character. The „band" nature of the states, manifested by several states with similar energy, is a consequence of the presence of 4 Ac molecules.

Type of the dominant electronic configuration	ΔE [eV]	f
DBT→DBT	1.618	0.281
Ac→DBT	2.139	0.029
	2.142	0.000
	2.188	0.000
	2.202	0.003
DBT→Ac	2.330	0.000
	2.335	0.000
	2.339	0.000
	2.377	0.014
DBT→DBT	2.654	0.000
	2.830	0.000
	2.885	0.000
	2.974	0.003
	3.178	0.001
	3.221	0.000
Ac→Ac	3.225	0.001
	3.227	0.001
	3.279	0.000
	3.281	0.003
DBT→DBT	3.320	0.033
Ac→Ac	3.341	0.000
	3.342	0.000
Ac→Ac DBT→DBT	3.369	0.148
Ac→Ac	3.379	0.000
	3.392	0.013
	3.403	0.000
Ac→Ac Ac→DBT	3.408	0.000
	3.413	0.013
	3.424	0.001
DBT→DBT	3.425	0.050
Ac→Ac	3.438	0.000
	3.444	0.006
	3.448	0.000
	3.450	0.003
	3.489	0.125
Ac→DBT	3.499	0.000

	3.530	0.018
	3.539	0.000
	3.557	0.014
	3.613	0.000
	3.622	0.018
	3.683	0.006
DBT→Ac	3.689	0.000
	3.711	0.000
	3.760	0.059
	3.765	0.000
	3.776	0.021

In the case of DBT/4Ac, the second photon, energy ~1.6 eV, following excitation of DBT molecule to its S_1 state (which is located 1.618 eV above the S_0), leads to the LE(DBT*) state of the energy 3.32 eV. This state is immersed in a dense distribution of excited states, described as Ac→Ac. In fact, we observed excited states where change of the distribution of charges following excitation concerns all 4 Ac molecules (see a visual example in Figure S3.13). Vibronic coupling leads to fluctuations of the energies of states, and, consequently, to their mixing. Charge-transfer dynamics was already modeled for the complex pentacene/C60 [S9], where it was based on the coupling of C−C bond-stretching and ring-breathings. Vibronic coupling between the LE(DBT*) and a manifold of (Ac→Ac) states can be considered as the reason of their mixing and evolution to the charge separated states.
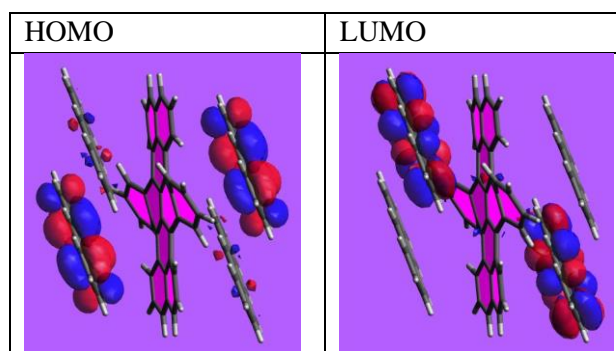
HOMO	LUMO

Figure S3.13: HOMO and LUMO orbitals for the Ac→Ac transition with the energy 3.279 eV.

The CT states between Ac molecules create charge carriers in Ac matrix, however we have not enough data to discuss this topic in more details.

Recovery of neutral DBT

Upon excitation of DBT and subsequent electron ejection from DBT and charge transfer to a matrix molecule (DBN or Ac), the positively charged hole remains temporarily on DBT. We have considered the question of the energy barrier between DBT^+-Ac and DBT-Ac^+ and possibility of hole transfer from DBT to Ac. In this respect, there are two possibilities, i.e., spontaneous filling of the hole and recovery of neutral DBT with the aid of optical excitation.

Case A: Spontaneous filling of the hole

Our calculations are analogous to polarization energy calculations in organic semiconductors [S10, S11], and the result is dependent on the number of host matrix molecules taken into consideration. Table S3.5 summarizes calculated energies for different numbers of Ac molecules in the unit cell.

Table S3.5: Energies of the systems where DBT is surrounded by different numbers of Ac molecules. Calculations were done with the ONIOM (B3LYP/3-21G:B3LYP/3-21G) method.

Number of Ac molecules	$E(DBT^+-Ac)$ [au]	$E(DBT-Ac^+)$ [au]	ΔE [eV]
1 Ac	-1988.3167	-1988.2628	1.4652
4 Ac	-3598.0882	-3598.0654	0.6217
36 Ac	-20764.8899	-20764.8888	0.0299

The calculated energy difference in case of DBN–36Ac is small (~0.03 eV). Ionization potential in case of Ac molecule is smaller than the ionization potential of DBN. Similar calculations performed for DBT surrounded by molecules of DBN led to the energy barrier ~0.9 eV, an order of magnitude bigger than for Ac.

Case B: Recovery of neutral DBT with the aid of optical excitation.

Table S3.6: Energies of excitation for isolated cation of DBT with 1 molecule of DBN, and with 4 Ac molecules. Calculations performed with the TDDFT/B3LYP/3-21G method.

DBT^+		$(DBT-DBN)^+$			$(DBT - 4\ Ac)^+$		
ΔE [eV]	f	ΔE [eV]	f	character	ΔE [eV]	f	character
0.927	0.092	1.061	0.006	DBN→DBT	0.472	0.000	Ac→DBT
1.706	0.062	1.245	0.031	DBT→DBT	0.479	0.000	Ac→DBT
1.913	0.256	1.523	0.010	DBN→DBT	0.583	0.022	Ac→DBT
		1.562	0.019	DBT→DBT	0.600	0.000	Ac→DBT
		1.807	0.347	DBT→DBT	1.102	0.055	DBT→DBT
		1.865	0.027	DBT→DBT	1.658	0.054	DBT→DBT
					1.774	0.000	Ac→DBT
					1.778	0.046	Ac→DBT
					1.866	0.084	Ac→DBT
					1.875	0.000	Ac→DBT

In a range of small energies, comparable to the energies of excitation used in the experiment, there are CT transitions, where an electron is transferred from Ac or DBN to DBT.
1.523 eV in the system DBT^+-DBN
1.778 eV in the system DBT^+-4Ac

These results suggest that recovery of neutral DBT happens with the aid of optical excitation.

Consistency of the model with experiments

We verify the consistency of our model with the following experimental observations:

- Illumination by the pump laser shifts the ZPLs almost continuously, and by up to several tens of GHz, with no significant broadening of the optical transition. This is consistent with our hypothesis that charges are trapped relatively far from the probed DBT molecule, so that each single-charge process gives rise to an undetectably small shift of the probed ZPL. The measured shift must result from the accumulation of many single-charge events at relatively large distances.

- The ZPL shift persists for long times, at least 24 h after the pump laser has been switched off. This indicates that the separated charges are far enough from each other that recombination by tunneling remains negligible on hours to days time scales. Such time scales require distances larger than tens of nm.

- The ZPL shift scales sub-linearly with power and can be fitted with a power law of time (eq. 1 of the main text). Power-law kinetics have been observed in the relaxation of charge distributions injected by electrodes in anthracene-based FETs. [S12] This observation supports our assignment of the ZPL shift to slowly varying charge distributions.

- The shift depends only weakly on the pump laser wavelength, with no clear effect of a resonance with DBT levels. This observation supports our assignment to a broad absorption or action spectrum, such as those of excited-state or molecular-ion absorption.

- The shift is observed both on dielectric and metallic substrates, indicating that the charge separation and trapping processes happen in the molecular material itself. The charges are not injected from non-organic materials outside the matrix.

The single-molecule time traces of resonant DBT molecules (Figure 3.1 and Figure 3.2.) give important hints as to local charge dynamics and electric fields. Instead of large discrete spectral jumps, the resonant DBT emitters appear to be continuously shifted for long periods of time by pump exposure. This suggests that many charge carriers contribute to the shift and that the separated charges do not reside in a close proximity of the probed DBT molecules. Furthermore, the long-term stability of the spectral lines after pump illumination points toward long recombination times and low tunneling rates of the charge carriers trapped in the matrix. Assuming the low tunneling rates, we can estimate a lower bound to the distance between separated charges of at least 20 nm.

We first considered direct two-photon excitation of matrix molecules (Ac and DBN) as the possible photoionization mechanism. However, the close-to-linear power dependence of the frequency shift, shown in Figure 3.2.a, rules out single-step, two-photon-induced

photoionization of the matrix. In both types of crystals, we observe background fluorescence whose spectrum shows that it originates from the pump-excited, non-resonant DBT molecules. This background also scales linearly with the excitation power (see SI). Finally, by using linearly polarized pump excitation on a well-oriented DBT:DBN single crystal, we verified that the intensity of the background fluorescence signal correlates with the magnitude of the spectral shift. As DBT cannot be ionized by a single pump or probe photon, we propose that DBT must be ionized via a cascade of two successive single-photon excitations (step A in Figure 3.5). Photoionization results in two charged molecules, DBT^+ and M^- (step B in Figure 3.5). This charge-separated state most likely does not exist for long periods of time. Under conditions of strong illumination, however, both the trapped electron and the hole on DBT are likely to migrate further away into the matrix, creating thus M^- and M^+ species with large separations. This conclusion is in line with our experimental observations. The latter step of photoinduced hole transport regenerates DBT to a photoactive state that can generate further separated electron-hole pairs (step C in Figure 3.5).

Charge separation in the matrix is most likely induced by several background chromophores. These are found in large amounts in the densely doped DBT:DBN crystal, but also in small numbers in the DBT:Ac NCX, e.g. most likely embedded at the nanocrystal surfaces or at imperfections. These background molecules probably exhibit broad optical transitions, thus do not readily appear in high-resolution spectra, and do not significantly affect the anti-bunching measurements. Because these molecules are not necessarily resonant with the probe and probably give rise to very broad optical lines, the process is expected to be nearly independent of the pump frequency, as shown in Figure3.2.c.

The ZPL spectral shits can be fitted with power laws, with a faster initial change that slows down in time (Figure 3.2). The spectral shift over time was also explained as consequent to charge transport in the guest-host system. [S13] Similar power-law behavior was reported for co-sublimated DBT:Ac crystals.[S12], in the presence of hole injection by gold electrodes in contact with the anthracene crystal. These authors observed that charges initially trapped inside the crystal were subsequently de-trapped via migration in the host matrix and tunneling through the dielectric substrate (or via simple charge recombination through a metallic substrate). The similar kinetics in both cases suggests that dispersive transport in the organic matrix is at work in both cases.

It is worth noting that, during the pump illumination, we sometimes do observe small spectral jumps giving rise to noise on top of the power-law trend. These stochastic fluctuations of static electric field might indicate discrete charge hopping events and therefore give an idea of their distance from the probed DBT molecule.

We have also considered other possible mechanisms that may take place during intense laser illumination. While light-induced single-molecule frequency shifts have already been reported in the literature [S14], the reported relatively weak shifts of about 600 MHz/W were reversible, non-tunable in time, and obtained under significantly stronger pump illumination. The authors ascribed the results to the combination of the beam absorption and ac-Stark effect [S15]. However,

tunable all-optical frequency shifts of single molecules, which persist long after switching off of the pump source, have never been reported for single-photon emitters.

References

(1) Hettich, C.; Schmitt, C.; Zitzmann, J.; Kühn, S.; Gerhardt, I.; Sandoghdar, V. Nanometer Resolution and Coherent Optical Dipole Coupling of Two Individual Molecules. Science **2002**, 298, 385−389. (2) Pototschnig, M.; Chassagneux, Y.; Hwang, J.; Zumofen, G.; Renn, A.; Sandoghdar, V. Controlling the Phase of a Light Beam with a Single Molecule. Phys. Rev. Lett. **2011**, 107, No. 063001.

(3) Wang, D.; Kelkar, H.; Martin-Cano, D.; Rattenbacher, D.; Shkarin, A.; Utikal, T.; Götzinger, S.; Sandoghdar, V. Turning a Molecule into a Coherent Two-Level Quantum System. Nat. Phys.**2019**, 15, 483−489.

(4) Orrit, M.; Bernard, J. Single Pentacene Molecules Detected by Fluorescence Excitation in a *p* -Terphenyl Crystal. *Phys. Rev. Lett*. **1990**, 65, 2716−2719.

(5) Basché, T.; Moerner, W. E.; Orrit, M.; Talon, H. Photon Antibunching in the Fluorescence of a Single Dye Molecule Trapped in a Solid. Phys. Rev. Lett. **1992**, 69, 1516−1519.

(6) Lounis, B.; Moerner, W. E. Single Photons on Demand from a Single Molecule at Room Temperature. Nature **2000**, 407, 491−493. (7) Nicolet, A. A. L.; Bordat, P.; Hofmann, C.; Kol'chenko, M. A.; Kozankiewicz, B.; Brown, R.; Orrit, M. Single Dibenzoterrylene Molecules in an Anthracene Crystal: Main Insertion Sites. ChemPhysChem **2007**, 8, 1929−1936.

(8) Lettow, R.; Rezus, Y. L. A.; Renn, A.; Zumofen, G.; Ikonen, E.; Götzinger, S.; Sandoghdar, V. Quantum Interference of Tunably Indistinguishable Photons from Remote Organic Molecules. Phys. Rev. Lett. **2010**, 104, 123605.

(9) Rezai, M.; Wrachtrup, J.; Gerhardt, I. Coherence Properties of Molecular Single Photons for Quantum Networks. Phys. Rev. X **2018**, 8, No. 031026.

(10) Troiani, F.; Ghirri, A.; Paris, M.; Bonizzoni, C.; Affronte, M. Towards Quantum Sensing with Molecular Spins. J. Magn. Magn. Mater. **2019**, 491, 165534.

(11) Tian, Y.; Navarro, P.; Orrit, M. Single Molecule as a Local Acoustic Detector for Mechanical Oscillators. Phys. Rev. Lett. **2014**, 113, 135505.

(12) Lombardi, P.; Ovvyan, A. P.; Pazzagli, S.; Mazzamuto, G.; Kewes, G.; Neitzke, O.; Gruhler, N.; Benson, O.; Pernice, W. H. P.; Cataliotti, F. S.; Toninelli, C. Photostable Molecules on Chip: Integrated Sources of Nonclassical Light. ACS Photonics **2018**, 5, 126−132.

(13) Türschmann, P.; Rotenberg, N.; Renger, J.; Harder, I.; Lohse, O.; Utikal, T.; Götzinger, S.; Sandoghdar, V. Chip-Based All-Optical Control of Single Molecules Coherently Coupled to a Nanoguide. Nano Lett. **2017**, 17, 4941−4945.

(14) Rattenbacher, D.; Shkarin, A.; Renger, J.; Utikal, T.; Götzinger, S.; Sandoghdar, V. Coherent Coupling of Single Molecules to On- chip Ring Resonators. New J. Phys. **2019**, 21, No. 062002.

(15) Colautti, M.; Lombardi, P.; Trapuzzano, M.; Piccioli, F. S.; Pazzagli, S.; Tiribilli, B.; Nocentini, S.; Cataliotti, F. S.; Wiersma, D. S.; Toninelli, C. A 3D Polymeric Platform for Photonic Quantum Technologies. Adv. Quantum Technol. **2020**, 3, 2000004.

(16) Aumaitre, C.; Morin, J.-F. Polycyclic Aromatic Hydrocarbons as Potential Building Blocks for Organic Solar Cells. Chem. Rec. **2019**, 19, 1142−1154.

(17) Yang, B.; Trebbia, J.-B.; Baby, R.; Tamarat, P.; Lounis, B. Optical Nanoscopy with Excited State Saturation at Liquid Helium Temperatures. Nat. Photonics **2015**, 9, 658−662.

(18) Wild, U. P.; Güttler, F.; Pirotta, M.; Renn, A. Single Molecule Spectroscopy: Stark Effect of Pentacene in p-Terphenyl. Chem. Phys. Lett. **1992**, 193, 451−455.

(19) Orrit, M.; Bernard, J.; Zumbusch, A.; Personov, R. Stark Effect on Single Molecules in a Polymer Matrix. Chem. Phys. Lett. **1992**, 196, 595−600.

(20) Tamarat, P.; Lounis, B.; Bernard, J.; Orrit, M.; Kummer, S.; Kettner, R.; Mais, S.; Basché, T. Pump-Probe Experiments with a Single Molecule: ac-Stark Effect and Nonlinear Optical Response. Phys. Rev. Lett. **1995**, 75, 1514−1517.

(21) Schädler, K.; Ciancico, C.; Pazzagli, S.; Lombardi, P.; Bachtold, A.; Toninelli, C.; Reserbat-Plantey, A.; Koppens, F. H. L. Electrical Control of Lifetime-Limited Quantum Emitters Using 2D Materials. Nano Lett. **2019**, 19, 3789−3795.

(22) Moradi, A.; Ristanovic', Z.; Orrit, M.; Deperasin'ska, I.; Kozankiewicz, B. Matrix-Induced Linear Stark Effect of Single Dibenzoterrylene Molecules in 2,3-Dibromonaphthalene Crystal. ChemPhysChem **2019**, 20, 55−61.

(23) Fiset-Cyr, A.; Dalacu, D.; Haffouz, S.; Poole, P. J.; Lapointe, J.; Aers, G. C.; Williams, R. L. In-Situ Tuning of Individual Position-Controlled Nanowire Quantum Dots via Laser-Induced Intermixing. Appl. Phys. Lett. **2018**, 113, No. 053105.

(24) Takahashi, M.; Syafawati Humam, N.; Tsumori, N.; Saiki, T.; Regreny, P.; Gendry, M. Local Control of Emission Energy of Semiconductor Quantum Dots Using Volume Expansion of a Phase-Change Material. Appl. Phys. Lett. **2013**, 102, No. 093120.

(25) Grim, J. Q.; Bracker, A. S.; Zalalutdinov, M.; Carter, S. G.; Kozen, A. C.; Kim, M.; Kim, C. S.; Mlack, J. T.; Yakes, M.; Lee, B.; Gammon, D. Scalable in Operando Strain Tuning in Nanophotonic Waveguides Enabling Three-Quantum-Dot Superradiance. Nat. Mater. **2019**, 18, 963−969.

(26) Lombardi, P.; Trapuzzano, M.; Colautti, M.; Margheri, G.; Degiovanni, I. P.; Lo'pez, M.; Kück, S.; Toninelli, C. A Molecule- Based Single-Photon Source Applied in Quantum Radiometry. Adv. Quantum Technol. **2020**, 3, 1900083.

(27) Pazzagli, S.; Lombardi, P.; Martella, D.; Colautti, M.; Tiribilli, B.; Cataliotti, F. S.; Toninelli, C. Self-Assembled Nanocrystals of Polycyclic Aromatic Hydrocarbons Show Photostable Single-Photon Emission. ACS Nano **2018**, 12, 4295−4303.

(28) Nicolet, A. A. L.; Kol'chenko, M. A.; Hofmann, C.; Kozankiewicz, B.; Orrit, M. Nanoscale Probing of Charge Transport in an Organic Field-Effect Transistor at Cryogenic Temperatures. Phys. Chem. Chem. Phys. **2013**, 15, 4415−4421.

(29) Silinsh, E. A. Organic Molecular Crystals: Their Electronic States, 1st ed.; Springer-Verlag: Berlin, Heidelberg, **1980**.

(30) Karl, N. In Festkörperprobleme XIV; Queisser, H. J., Ed.; Springer: Berlin, Heidelberg, **1974**; pp 261−290.

(31) Hoesterey, D.; Letson, G. The Trapping of Photocarriers in Anthracene by Anthraquinone, Anthrone and Naphthacene. J. Phys. Chem. Solids **1963**, 24, 1609−1615.

(32) Moerner, W. E.; Silence, S. M. Polymeric Photorefractive Materials. Chem. Rev. **1994**, 94, 127−155.

(33) Stadtmüller, B.; Emmerich, S.; Jungkenn, D.; Haag, N.; Rollinger, M.; Eich, S.; Maniraj, M.; Aeschlimann, M.; Cinchetti, M.; Mathias, S. Strong Modification of the Transport Level Alignment in Organic Materials after Optical Excitation. Nat. Commun. **2019**, 10, 1470.

(34) Causa', M.; Ramirez, I.; Martinez Hardigree, J. F.; Riede, M.; Banerji, N. Femtosecond Dynamics of Photoexcited C60 Films. J.

Phys. Chem. Lett. **2018**, 9, 1885−1892.

(35) Hahn, T.; Tscheuschner, S.; Saller, C.; Strohriegl, P.; Boregowda, P.; Mukhopadhyay, T.; Patil, S.; Neher, D.; Bassler, H.; Köhler, A. Role of Intrinsic Photogeneration in Single Layer and Bilayer Solar Cells with C60 and PCBM. J. Phys. Chem. C **2016**, 120, 25083−25091.

(36) Schwoerer, M.; Wolf, H. C. Organic Molecular Solids, 1st ed.; Wiley-VCH: Weinheim, **2008**.

(37) Malloci, G.; Joblin, C.; Mulas, G. On-line Database of the Spectral Properties of Polycyclic Aromatic Hydrocarbons. Chem. Phys. 2007, 332, 353−359.

Supplementary References

(S1) S. Pazzagli, P. Lombardi, D. Martella, M. Colautti, B. Tiribilli, F. S. Cataliotti, C. Toninelli, ACS Nano 2018, 12, 4295–4303.

(S2) R. C. Schofield, K. D. Major, S. Grandi, S. Boissier, E. A. Hinds, A. S. Clark, J. Phys. Commun. 2018, 2, 115027.

(S3) A. Nicolet, P. Bordat, C. Hofmann, M.A. Kol'chenko, B. Kozankiewicz, R. Brown and M. Orrit, Single dibenzoterrylene molecules in an anthracene crystal. Main insertion sites, ChemPhysChem 8 (2007) 1929-1936.

(S4) A. Moradi, Z. Ristanovic, M. Orrit, I. Deperasińska, B. Kozankiewicz, Matrix-induced Linear Stark Effect of Single Dibenzoterrylene Molecules in 2,3-Dibromonaphthalene Crystal, ChemPhysChem (2019)

(S5) N. Karl, Festkörperprobleme IX 1974, 261–290.

(S6) E. A. Silinsh, Organic Molecular Crystals: Their Electronic States, Springer, 1980.

(S7) Z. S. Sadeq, Rodrigo A. Muniz, and J. E. Sipe, Phys. Rev. Materials 2, 075202 (2018).

(S8) A. Nicolet, C. Hofmann, M. Kol'chenko, B. Kozankiewicz, and M. Orrit, Single dibenzoterrylene molecules in an anthracene crystal. I. Spectroscopy and photophysics, ChemPhysChem 8 (2007) 1215-1220.

(S9) S. Joseph, M. Kumar Ravva, and J.-L. Bredas, Charge-Transfer Dynamics in the Lowest Excited State of a Pentacene−Fullerene Complex: Implications for Organic Solar Cells, J. Phys. Chem. Lett. 2017, 8, 5171−5176.

(S10) J. E. Norton, J.-L. Bredas, Polarization Energies in Oligoacene Semiconductor Crystals, J. Am. Chem. Soc. 2008, 130, 12377–12384.

(S11) F. Castet, P. Aurel, A. Fritsch, L. Ducasse, D. Liotard, M. Linares, J. Cornil, and D. Beljonne, Electronic polarization effects on charge carriers in anthracene: A valence bond study, Phys. Rev. B, 2008, 77, 115210.

(S12) Nicolet, A. A. L., Kol'chenko, M. A., Hofmann, C. Kozankiewicz, B. & Orrit, M. Nanoscale probing of charge transport in an organic field-effect transistor at cryogenic temperatures. Phys. Chem. Chem. Phys.15, 4415–4421 (2013).

(S13) Scher, H. & Montroll, E. W. Anomalous transit-time dispersion in amorphous solids, Phys. Rev. B12,2455–2477 (1975).

(S14) Plakhotnik T., Walser D., Renn A. & Wild U. P., Light induced single molecule frequency shift, Phys. Rev. Lett. 77, 5365–5368 (1996).

(S15) P. Tamarat, B. Lounis, J. Bernard, M. Orrit, S. Kummer, R. Kettner, S. Mais, T. Basché, Phys. Rev. Lett. 1995, 75, 1514–1517.